Global and Planetary Change 162 (2018) 101–119

Contents lists available at ScienceDirect

Global and Planetary Change

journal homepage: www.elsevier.com/locate/gloplacha

The Eocene-Oligocene transition in the North Alpine Foreland Basin and subsequent closure of a Paratethys gateway

A. van der Boon[a,*], A. Beniest[b], A. Ciurej[c], E. Gaździcka[d], A. Grothe[a], R.F. Sachsenhofer[e], C.G. Langereis[a], W. Krijgsman[a]

[a] Paleomagnetic Laboratory 'Fort Hoofddijk', Utrecht University, Budapestlaan 17, Utrecht, The Netherlands
[b] Sorbonne Universités, UPMC University Paris 06, CNRS, Institut des Sciences de la Terre de Paris (ISTeP), 4 Place Jussieu, 75005 Paris, France
[c] Pedagogical University, Podchorążych 2, 30-084 Kraków, Poland
[d] Państwowy Instytut Geologiczny – Państwowy Instytut Badawczy, ul. Rakowiecka 4, 00-975 Warszawa, Poland
[e] Department of Applied Geosciences and Geophysics, Chair of Petroleum Geology, Montanuniversitaet Leoben, Peter-Tunner-Strasse 5, Leoben A-8700, Austria

ARTICLE INFO

Keywords:
Eocene-Oligocene transition
Molasse
Magnetostratigraphy
Paratethys
Biostratigraphy
Marine-continental transition

ABSTRACT

During the Eocene-Oligocene transition (EOT), a major palaeoenvironmental change took place in the Paratethys Sea of central Eurasia. Restricted connectivity and increased stratification resulted in wide-spread deposition of organic-rich sediments which nowadays make up important hydrocarbon source rocks. The North Alpine Foreland Basin (NAFB) was a major gateway of the Paratethys Sea to the open ocean during the Eocene, but the age of closure of this gateway is still uncertain.

The Ammer section in southern Germany documents the shallowing of this connection and subsequent disappearance of marine environments in the NAFB, as reflected in its sedimentary succession of turbidites to marls (Deutenhausen to Tonmergel beds), via coastal sediments (Baustein beds) to continental conglomerates (Weißach beds). Here, we apply organic geochemistry and date the lithological transitions in the Ammer section using integrated stratigraphy, including magnetostratigraphy and biostratigraphy. Nannoplankton and dinocyst results can be reconciled when dinoflagellate species *Wetzeliella symmetrica* is of late Eocene age. Our magnetostratigraphy then records C13r-C13n-C12r and allows calculation of sediment accumulation rates and estimation of ages of lithological transitions.

We show that the shallowing from turbiditic slope deposits (Deutenhausen beds) to shelf sediments (Tonmergel beds) coincides with the Eocene-Oligocene boundary at 33.9 Ma. The transition to continental sediments is dated at ca. 33.15 Ma, significantly older than suggested by previous studies. We conclude that the transition from marine to continental sediments drastically reduced the marine connection through the western part of the NAFB and influenced the oxygen conditions of the Paratethys Sea.

1. Introduction

During the early Oligocene, the epicontinental Paratethys Sea covered large areas of central Europe, southern Russia and central Asia (Akhmet'ev, 2011; Rögl, 1998). The Oligocene deposits in the highly restricted Paratethys basins represent a long-term phase of (episodically) oxygen-poor conditions that continued well into the Miocene for the Eastern Paratethys. During this time, thick successions of organic-rich shales (e.g. Maikop Series, Johnson et al., 2010; Popov et al., 2008) were deposited in the Eastern Paratethys. For example, up to 2 kilometres thick Maikop sediments can be found in the Western Black Sea (Georgiev, 2012), while in Azerbaijan, 1.2 kilometres of Maikop sediments are present onshore, increasing to up to 3 km offshore (Hudson et al., 2008). These shales form a major source rock for hydrocarbon exploitation in central Europe, the Black Sea and Caspian Sea (e.g. Sachsenhofer and Schulz, 2006; Sachsenhofer et al., 2017). In the Central Paratethys domain, a conspicuous change from Eocene carbonates to Oligocene black shales is reported from the Austrian Molasse Basin (Schulz et al., 2005). Connectivity between the Paratethys and the open ocean must have been very limited and stable to allow for such a long period (15–20 Myr; Hudson et al., 2008) of oxygen-poor conditions in the Eastern Paratethys, which requires severe water mass stratification to prevent mixing and ventilation of the bottom waters.

Inferred mechanisms for Paratethys sea retreat and consecutive

* Corresponding author at: University of Liverpool, Oliver Lodge Laboratory, Liverpool L7 7BD, UK
E-mail addresses: a.vanderboon@uu.nl (A. van der Boon), anouk.beniest@etu.upmc.fr (A. Beniest), aciurej@up.krakow.pl (A. Ciurej), egaz@pgi.gov.pl (E. Gaździcka), a.grothe@uu.nl (A. Grothe), reinhard.sachsenhofer@unileoben.ac.at (R.F. Sachsenhofer), c.g.langereis@uu.nl (C.G. Langereis), w.krijgsman@uu.nl (W. Krijgsman).

https://doi.org/10.1016/j.gloplacha.2017.12.009
Received 4 April 2017; Received in revised form 10 November 2017; Accepted 6 December 2017
Available online 16 December 2017

basin restriction are large scale tectonic movements in the Alpine region (e.g. Rögl, 1998; Sissingh, 2006) and the Arabia-Eurasia convergence zone (e.g. Cowgill et al., 2016), as well as climatically induced eustatic sea-level changes (e.g. Schulz et al., 2005). Disentangling climatic from tectonic forcing processes is a prerequisite for understanding the mechanisms driving widespread deposition of anoxic shales in the Paratethys domain. This requires a robust time frame for the Eocene-Oligocene deposits of the Paratethys, which is currently lacking, because of generally poor stratigraphic constraints. The scarcity of volcanic ash-layers and problems with biostratigraphic marker species in these oxygen-poor environments further complicate the understanding of the mechanisms that drove the environmental changes in the Paratethys. Magnetostratigraphy is a tool that can circumvent these issues if a section is continuous, yields sufficient magnetic reversals and is characterised by relatively stable sediment accumulation rates. Moreover, the original magnetic signal needs to be preserved (Langereis et al., 2010). Long and complete sedimentary successions that straddle the EOT are necessary to resolve the respective roles of eustatic sea level changes and tectonics on Paratethys restriction, but these sections are quite rare, as the Oligocene deposits of Paratethys are often very soft and tectonically affected.

The North Alpine Foreland Basin (NAFB) was one of the few basins that connected the Paratethys Sea to open marine waters. The western part of the NAFB was part of the Western Paratethys domain and shows a conspicuous change from late Eocene marine towards early Oligocene continental deposits (Kempf and Pross, 2005). This region documents the progressive closure of the marine Paratethys connection via the NAFB, the Molasse Basin of Switzerland and the Rhône Basin of France to the proto-Mediterranean. The marine-continental change in the western NAFB corresponds to the transition from the Lower Marine Molasse (Untere Meeresmolasse: UMM in German) to the Lower Freshwater Molasse (Untere Süßwasser Molasse: USM in German). The eastern part of the NAFB remained marine throughout the Oligocene and there are no USM deposits found east of Munich (Doppler et al., 2005). For practical reasons, this paper will follow the German terminology.

In the western NAFB, an exceptionally long (> 1.5 km) continuous succession of deposits that show a progression from a marine (UMM) to continental (USM) depositional environment is located along the Ammer River in southern Germany (47.66°N, 10.99°E; Fig. 1). The Ammer section starts with the Deutenhausen beds, consisting mainly of sandy turbidites (Fig. 2; Dohmann, 1991), which gradually merges into the Tonmergel beds, a long sequence of primarily grey marls. These marls are overlain by sandy deposits of the Baustein beds and continental conglomerates of the Weißach beds; the latter correspond to the lowermost deposits of the USM.

In this paper, we use an integrated stratigraphic approach, combining magnetostratigraphy with various biostratigraphic (dinoflagellate cysts, calcareous nannofossils) proxies to date the onset and termination of the marine deposits (Tonmergel marls) in the western NAFB. Hence, we will develop a magneto-biostratigraphic time frame for the upper part of the marine UMM (Deutenhausen, Tonmergel and Baustein beds) and the transition to the continental USM (Weißach beds) in the Ammer section, and discuss the relation of the observed lithological and palaeoenvironmental changes to global eustatic sea-level changes and/or regional tectonic phases.

1.1. Geologic background

During the Eocene, central Eurasia was covered by the well-oxygenated and predominantly shallow marine peri-Tethys Sea, which had open marine connections to the Tethys Ocean, the Arctic Sea and the North Sea (see Fig. 1; Akhmetiev and Beniamovski, 2009; Popov et al., 2004; Rögl, 1999). The peri-Tethys started to retreat from the Tarim Basin of western China (e.g. Bosboom et al., 2014) in the early Bartonian (~41 Ma). The southern connections to the Tethys Ocean were closed sometime around the late Eocene by plate tectonic convergence in the Arabia-Iran-Eurasia zone and wide-spread volcanism in a large belt from Turkey to SE Iran (van der Boon et al., 2015; Vincent et al., 2005). The gateway between the West Siberian Sea and the Arctic Ocean was already closed during the Bartonian-Priabonian (Akhmetiev and Beniamovski, 2009). Late Eocene tectonic activity and climatic changes terminated the open marine environments of the peri-Tethys. This resulted in a highly restricted Paratethys Sea, which is marked by the presence of endemic fauna throughout the Paratethys (Laskarev, 1924). During the Oligocene, the main remaining Paratethys gateways were connections to the North Sea Basin through central Europe (Poland-Germany-Denmark connection) and via the North Alpine foreland basin that connected to the North Sea via the Upper Rhine Graben and the proto-Mediterranean via the Rhône graben (e.g. Popov et al., 2004). No connection to the eastern Mediterranean through the Bosporus is to be expected, as the North Aegean Sea, through which the Sea of Marmara connects to the Mediterranean Sea, was not yet fully developed in the Oligocene. Only after a second extension phase during the Miocene did the North Aegean Sea fully expand (Beniest et al., 2016). The connection of the Paratethys to the Mediterranean southeast of the Alps is most likely closed during the Rupelian, as Schmiedl et al. (2002) report an isolation of the Paratethys from the open ocean for sediments

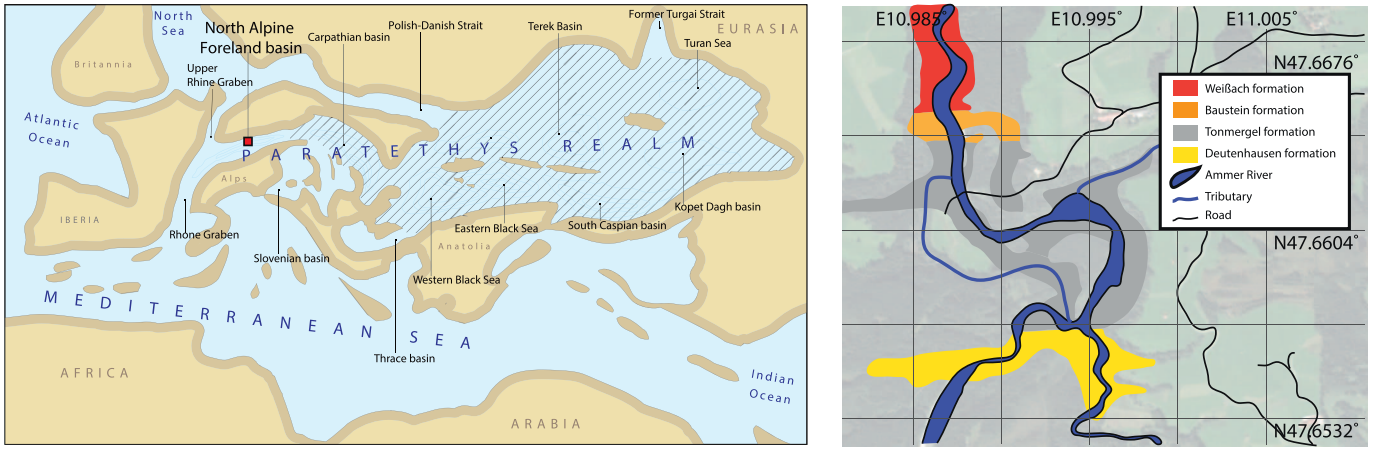

Fig. 1. Left: Location of the section (red square) and rough extent of the Paratethys sea around the Eocene-Oligocene transition (modified after Palcu et al., in prep.). Right: aerial photograph of the section with an overlay of the geologic map of Bayersoien. (For interpretation of the references to colour in this figure legend, the reader is referred to the web version of this article.)
(Modified after Höfle and Kuhnert, 1969.)

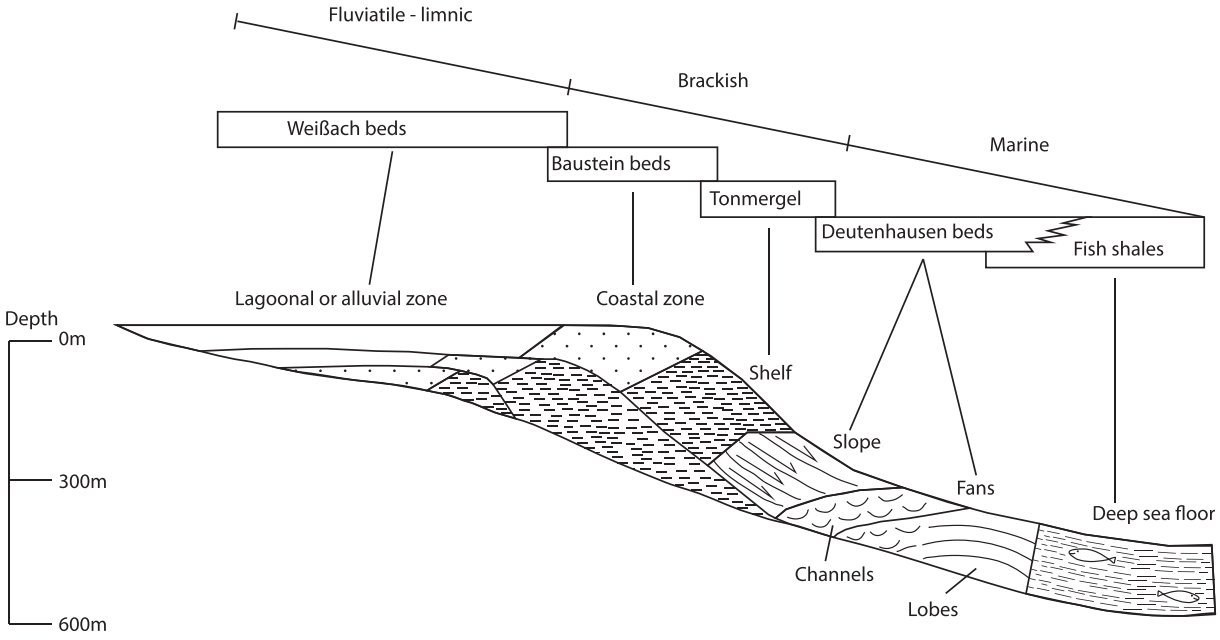

Fig. 2. Diagram of depositional depth of different lithologic units along the Ammer river. (After Dohmann, 1991.)

in the Slovenian Basin. After a period of relative tectonic quiescence, deformation in the Alpine region became influenced by the late Eocene-early Oligocene Pyrenean orogenic phase, after which a prolonged period of basin subsidence and deposition followed (Sissingh, 2006). The NAFB experienced flexural subsidence due to the north-advancing Alpine nappes, and was gradually filled up by molasse deposits (Berger et al., 2005b; Kuhlemann and Kempf, 2002; Reichenbacher et al., 2004). The influence of the Alpine orogeny is not synchronous throughout the whole NAFB, as the collision propagated westwards towards the Western Alps and eastwards towards the Carpathians (Sissingh, 2006). Although sedimentation in different parts of the Alpine foreland basin and the Upper Rhine Graben shows similar progressions from well-oxygenated foraminiferal marls to clays (e.g. Sissingh, 1998, 2001), many different names for lithologic units are used. We refer to the papers of Berger et al. (2005a, 2005b) for a detailed description and discussion. The molasse deposits of the western NAFB are made up of two transgressive-regressive megasequences, which are mostly derived from the erosion of Alpine nappes (e.g. Diem, 1986). The oldest molasse deposits belong to the UMM, which is a transgressive sequence. The UMM is followed by the regressive sequence of the USM (Diem, 1986), although in some areas a transitional facies between the UMM and USM has been observed, known as the Lower Brackish Molasse (UBM), or Cyrena beds (Kempf and Pross, 2005; Reichenbacher et al., 2004). A second transgressive-regressive sequence contains the lower to middle Miocene Upper Marine Molasse (Obere Meeresmolasse, OMM) and Upper Freshwater Molasse (Obere Süßwasser Molasse, OSM) (Doppler et al., 2005; Kempf and Matter, 1999).

1.2. The UMM-USM transition in the Ammer section (Germany)

The section along the Ammer River in the North Alpine Foreland Basin records the first transgressive-regressive sequence (UMM to USM). Here, the Deutenhausen, Tonmergel and Baustein beds make up the Lower Marine Molasse (UMM) sequence, while the USM is represented by the Weißach beds (Diem, 1986) (Fig. 1). For detailed sedimentary descriptions and interpretations, we refer to the studies of Diem (1986); Dohmann (1991); Höfle and Kuhnert (1969); and Maurer et al. (2002).

The Deutenhausen beds are reported to overlie the (Eocene) Unternogg beds, which represents the uppermost unit of the flysch fill of the NAFB (Höfle and Kuhnert, 1969). They consist of a well-bedded intercalation of grey marls and fine to medium (often massive) sandstones with scour marks, bioturbation and organic material. Current transport in the sandstones all point to a northward direction. The deposits are interpreted as turbidite fans, as they show clear examples of Bouma sequences (Diem, 1986). Towards the top of the unit, the sandstone and marl layers become thicker. The Deutenhausen beds are interpreted as a slope deposit (Fig. 2) (Dohmann, 1991). Although the reported thickness in the area is ~600 m (Höfle and Kuhnert, 1969), only the upper 245 m of the Deutenhausen beds (47.654498° N, 10.995837° E) were sampled, as the lowermost part is not exposed along the Ammer river.

The overlying Tonmergel beds are almost 850 m thick and consists of grey to dark grey marls, with some sand layers in its lowermost part. The Tonmergel is interpreted as a shelf deposit (Dohmann, 1991). At a stratigraphic level of ~490 m, synsedimentary deformation has affected the marls over a very short interval, and an intensely slumped sand lens stands out in the middle of the river (around 47.659458°N, 10.996305°E). The top of the Tonmergel beds also shows synsedimentary deformation expressed by small slumps (visible near the canal wall at the hydroelectric power plant Kammerl). The uppermost part contains many shells and shell fragments and the grainsize increases to silt and eventually sand. The boundary between the Tonmergel and the overlying Baustein beds are marked by the first thick sand bed (Höfle and Kuhnert, 1969).

The Baustein beds are a transitional facies between the marine Tonmergel and the continental Weißach beds, and consists mostly of silts, sands and marls, increasing in grainsize to conglomerates. Some parts could not be sampled, being on a steep cliff and/or covered by trees and soil. The lower part of the Baustein beds contains marine molluscs, while the upper part has brackish to continental mollusc fauna (Höfle and Kuhnert, 1969). In the middle part of the Baustein, cross-beds and wave ripples are observed, indicating a coastal depositional environment. The boundary with the overlying Weißach beds is placed on the first prominent conglomerate bed (47.665341°N, 10.986776°E) (Höfle and Kuhnert, 1969).

The Weißach beds consists of alternating marls, silts, sands and

conglomerates, with some conglomerates showing reddish colours. The beds are regarded as continental fan deposits and have a reported thickness of around 1 km (Höfle and Kuhnert, 1969). Only the lowermost 350 m were sampled for this study, but extension to younger deposits is possible, as there is at least another few hundred metres of outcrop accessible.

2. Methods

2.1. Palaeomagnetism

Samples were collected during two field campaigns in 2013 and 2015. Conventional palaeomagnetic cores (25 mm Ø) were collected using a gasoline-powered motor drill and oriented using a magnetic compass. Directions were corrected for a present day declination (IGRF) of 2–3°. Samples were cut into specimens of approximately 22 mm length. In total almost 570 specimens were subjected to thermal (195 specimens) and alternating field (AF) (373 specimens) demagnetisation. Thermal demagnetisation was performed in a magnetically shielded furnace to maximum temperatures of 400 °C, using temperature increments of 20–60 °C. Part of the samples that were treated with AF demagnetisation were heated to 150 °C to avoid alteration by a chemical remanent magnetisation (cf. Van Velzen and Zijderveld, 1995), although this did not result in difference in interpreted directions. AF demagnetisation was performed with steps of 4–10 mT using an in-house built robotized system (Mullender et al., 2016). After each demagnetisation step, the natural remanent magnetisation (NRM) was measured on a 2G Enterprise horizontal cryogenic magnetometer equipped with three DC SQUIDS (noise level 3×10^{-12} Am^2). The 'per component' protocol was used, in which demagnetisation using alternating fields is applied per axis, after which the sample is measured. This protocol is used to prevent gyroremanent magnetisation, which can occur if greigite is present in samples.

Results were calculated using principal component analysis (Kirschvink, 1980) on Zijderveld diagrams (Zijderveld, 1967), using the interpretation portal of the paleomagnetism.org website (Koymans et al., 2016). Declination and inclination angles were calculated for pre-tilt (TC) and post-tilt (NOTC) signals. We determined planes (great circles) for two components with overlapping blocking temperatures or coercivity. Lines and planes were determined following an eigenvector approach (Kirschvink, 1980). If we have both ChRM directions ('set-points') and great circles, we use the method of (McFadden and McElhinny, 1988) to determine great circle solutions. Mean directions were calculated using Fisher statistics (Fisher, 1953). Statistical treatment of data follows Deenen et al. (2011) and Tauxe et al. (2010).

Thermomagnetic runs were performed on powdered samples, using a modified horizontal translation Curie balance with a cycling field, usually 150–300 mT (Mullender et al., 1993). Six cycles of heating and cooling were performed, up to a temperature of 700 °C.

Samples were measured at room temperature for magnetic susceptibility, using the AGICO KLY-3 Kappabridge. Susceptibility was normalized for the mass of the samples. Variations in susceptibility can be a measure for variations in climate, environment or detrital input (Ellwood et al., 2000; Hay, 1996, 1998), as these variations can lead to change in diagenetic conditions (e.g. Da Silva et al., 2012), reflected in different lithologies in the section.

The section was logged on a scale of ~10 cm. A detailed log with all the samples and sample levels is supplied in the Supplementary information (Fig. S1).

2.2. Biostratigraphy

2.2.1. Nannoplankton

Smear slides of fourteen samples of marls and claystones were studied for nannoplankton biostratigraphy, following the standard techniques described by Perch-Nielsen (1985a) and Bown and Young (1998). Slides were observed under an OLYMPUS BH2 light microscope with cross polarised light and phase contrast illumination, at 900 × and 1800 × magnification. The standard scheme of Martini (1971) was adopted for this study.

2.2.2. Coccolith limestones

Ten thin sections of laminated coccolith limestones were studied, using a Zeiss Axioskop 50 (transmitted light) polarizing microscope, equipped with a digital camera (Canon Power Shot A640). Three thin sections were studied using the scanning electron microscope (SEM): FEI Nova NanoSEM 200, at low vacuum, and voltage 15 to 20 kV on non-coated samples. Various modes of observation were used: charge contrast imaging (CCI) and back-scattered electrons (BSE). The SEM-BSE mode allows determination of the chemical composition of components. The SEM-CCI mode was used to study of the anatomical details of calcareous nannofossils. More technical details are given in Ciurej (2010). The samples are stored at the Institute of Geography, Pedagogical University of Cracow, Poland.

2.2.3. Dinoflagellate cysts

In total, 19 samples from the Ammer section were processed for palynological purposes. Sample processing followed standard palynological techniques of the Laboratory for Palaeobotany and Palynology (LPP), Utrecht University, The Netherlands (e.g. Brinkhuis et al., 2003). In short, ~5–20 g of oven-dried (60 °C) material was crushed, weighed and one tablet with a known amount of *Lycopodium clavatum* spores was added for semi-quantitative estimates. The sediments were then treated with HCl (30%) and HF (38%) to remove the carbonates and silicates, respectively. The remaining solution was sieved using a 250 and 15 μm sieve; the remaining fraction was mounted on a slide with glycerine jelly. Palynological analyses were performed using a light microscope at 400 × magnification. Taxonomy follows that cited in Fensome (2004).

2.3. Organic geochemistry

Samples of the Deutenhausen, Tonmergel and Baustein beds were analysed for organic geochemistry. These analyses were focused on the most fine grained and organic rich (estimated based on dark colours) deposits. As the Weißach beds contains little fine grained clayey layers, no samples of this beds were analysed. All samples were analysed in duplicate for total sulphur (S), total carbon (TC), and total organic carbon (TOC, after acidification of samples to remove carbonate) using an Eltra Helios C/S analyser. TC and TOC contents were used to calculate calcite equivalent percentages ($Calc_{equ}$ = [TC − TOC] ∗ 8.333). Pyrolysis measurements were performed using a "Rock-Eval 6" instrument. S2 (mg HC/g rock) values were used to calculate the Hydrogen index (HI = 100 × S2/TOC [mg HC/g TOC]; (Espitalié et al., 1977)). The temperature of maximum generation of hydrocarbons during pyrolysis (Tmax) was recorded as a maturity parameter.

3. Results

3.1. Palaeomagnetism

Susceptibility of the samples is in the range of 3×10^{-9}–5×10^{-7} m^3/kg, and is lower and more variable in the top of the Baustein beds and the Weißach beds, when compared to the Deutenhausen and Tonmergel beds. Curie balance results (see Fig. 3) show that magnetisation of all samples gradually decreases when heating, with reversible behaviour up to ~400 °C. Each of the samples shows a significant increase in total magnetisation from around 400 °C to around 500 °C, after which the total magnetisation further decreases, and is fully removed around 580 °C.

The decrease in magnetisation up to 400 °C is often indistinguishable from a paramagnetic curve according to Curie's law. However, in some cases, the decrease shows a typical signature for the breakdown of

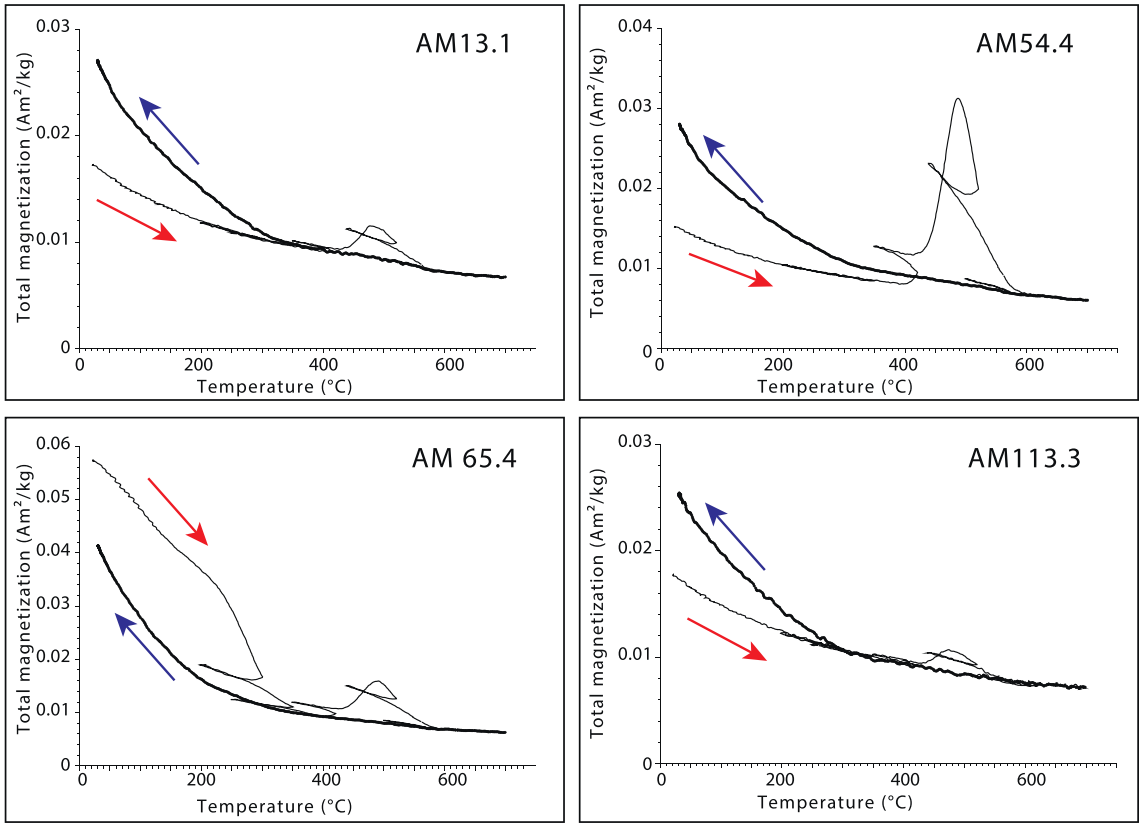

Fig. 3. Thermomagnetic runs using a Curie balance of different levels of claystones. Red arrows indicate heating lines, blue arrows indicate cooling lines. (For interpretation of the references to colour in this figure legend, the reader is referred to the web version of this article.)

iron sulphides. For example, sample AM65.4 shows irreversible behaviour before 400 °C and full decay around 350 °C, indicating the presence of greigite.

The increase in magnetisation above 400 °C is caused by the oxidation of the non-magnetic iron sulphide pyrite (FeS_2), which converts to magnetite around this temperature. The magnetite is subsequently fully demagnetised at 580 °C. The formation of magnetite above 400 °C causes erratic behaviour in the thermal demagnetisations, so demagnetisation was performed up to this temperature.

Examples of representative Zijderveld diagrams are shown in Fig. 4. Many samples show straightforward demagnetisation behaviour, with samples showing a low temperature/low coercivity component up to 150 °C or 15 mT. A high temperature/high coercivity component is generally isolated between ~200–340 °C or 20–60 mT. However, samples that have low intensities (less than ~100 μA/m) frequently show erratic behaviour after 45mT with AF demagnetisation, and above ~360 °C with thermal demagnetisation. Most samples demagnetise thermally up to temperatures of around 380 °C. Occasionally, samples (mainly within the Tonmergel beds) show behaviour that is typical for greigite, i.e. development of a gyroremanent magnetisation (GRM; Dankers and Zijderveld, 1981) upon application of alternating fields higher than 30–45 mT. These samples (e.g. AM50.1A; see Fig. 4 with Zijderveld examples) acquire a random magnetisation component, which grows above 45 mT. This is obvious from the intensity plot, which shows increasing intensity at higher demagnetisation steps. Only the steps below 40mT show normal or reversed polarities. Part of the samples, mainly in the top of the section, shows an increase in intensity and random behaviour from about 260 °C. These samples are interpreted using the demagnetisation steps from 200 to 260 °C.

Due to the near-vertical orientation of the beds, present day field (PDF) overprints are easily distinguished from pre-tilt signals.

Based on the demagnetisation results, we assigned a quality factor to the interpreted components. High quality samples in general show relatively straight demagnetisation lines towards the origin, and plotted vectors are anchored to the origin of the Zijderveld diagrams (Fig. 4).

Low quality samples often do not decrease towards the origin, and were interpreted without anchoring to the origin (Fig. 4). Although the maximum angle of deviation (MAD) for low quality samples is generally high, polarities could still be confidently assessed. Samples of which no polarity could be assigned are included in the online Appendix (.dir files), but are not plotted in the interpretation of the magnetostratigraphic pattern. Some samples show consistent normal directions before tectonic correction, and are clearly the result of overprinting by a post-tilt signal.

Fig. 5 shows a simplified log of the section, together with the interpreted directions after tilt correction (TC) of all samples with their assigned quality. Clear overprints are visible mostly in the upper, sandier part of the section, and high quality directions are scarcer. The bottom part of the section (0–490 m) shows reversed polarities, followed by an interval (490–1260 m) of normal polarities. The top part of the section (1260–1620 m) is again reversed. Occasionally, low quality samples or great-circle solutions show opposing polarities from the dominant polarity. These are not taken into account for establishing the polarity pattern. At a few levels, also high quality samples show an opposing polarity, but since they are usually close to, or within intervals with low quality data, great-circles and overprints, we consider them outliers. Moreover, thanks to the large amount of samples, we find primarily consistent polarities with high quality data in these same stratigraphic levels.

Characteristic magnetisation directions and associated VGPs for all data, as well as only high quality data are shown in Fig. 6. The mean of the high quality reversed directions (D = 10.2° ± 3.0, I = 58.8° ± 3.3) is not antipodal to the mean of the high quality normal directions (D = 19.5° ± 3.0, I = 54.4° ± 2.5). The

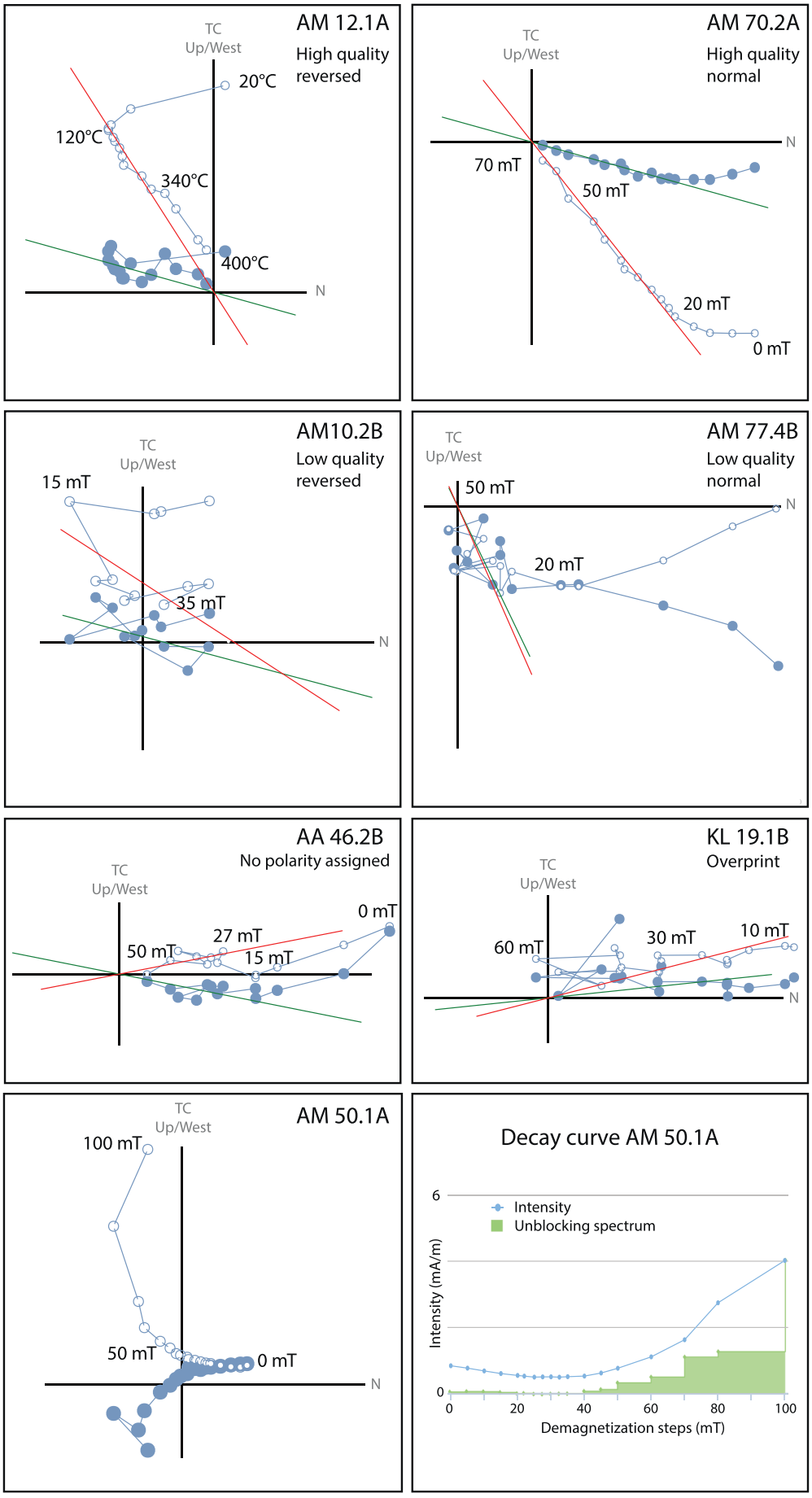

Fig. 4. Examples of different qualities of Zijderveld diagrams and a decay curve for sample AM50.1A, containing greigite. TC is tilt-corrected. Closed (open) symbols denote projection on the horizontal (vertical) plane. Red (green) lines indicate the projections of the characteristic remanent magnetisation (ChRM) directions on the vertical (horizontal) plane. Decay curve shows an increase upon AF demagnetisation due to the presence of greigite. (For interpretation of the references to colour in this figure legend, the reader is referred to the web version of this article.)

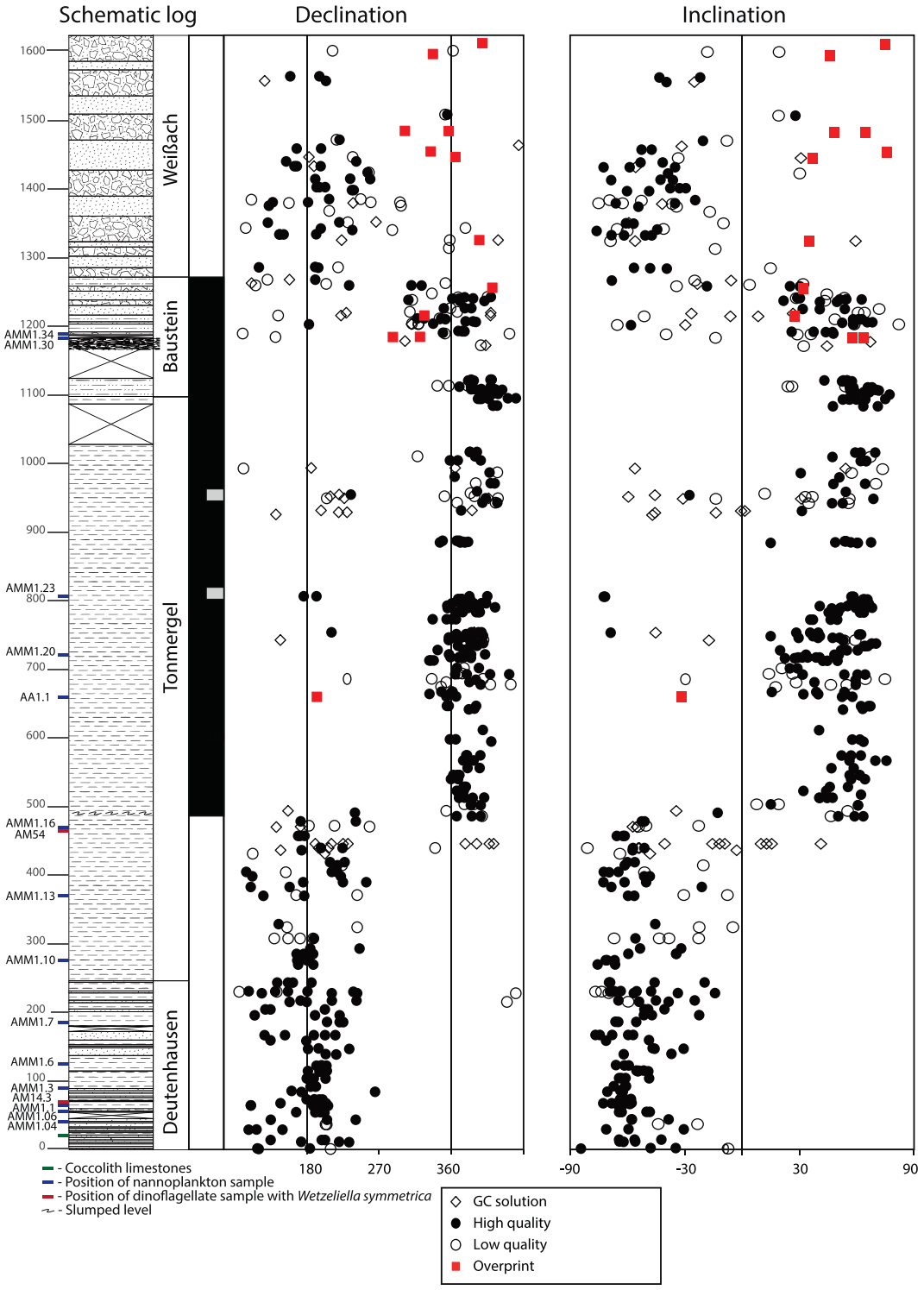

Fig. 5. Interpretation of ChRM declinations and inclinations with quality of components and polarity interpretation (white – reversed, black – normal). Great circle solutions for reversed samples are marked with a diamond. Samples that showed an overprint are in red and are shown without tectonic correction. Position of nannoplankton samples and coccolith limestones is shown in the log. (For interpretation of the references to colour in this figure legend, the reader is referred to the web version of this article.)

declinations significantly differ, by approximately 10°. The inclinations are within error, although the normal inclination is slightly shallower. Indeed, the coordinate bootstrap reversal test (Tauxe et al., 2010) is negative.

3.2. Biostratigraphy

3.2.1. Nannoplankton

Calcareous nannoplankton was studied in 14 samples of the Ammer profile, results of which are summarised in Table 1. Photographs of nannoplankton are shown in Fig. 7. The majority of examined samples contain abundant but inhomogeneous nannofossil assemblages. Numerous coccoliths are reworked from older sediments, both from the

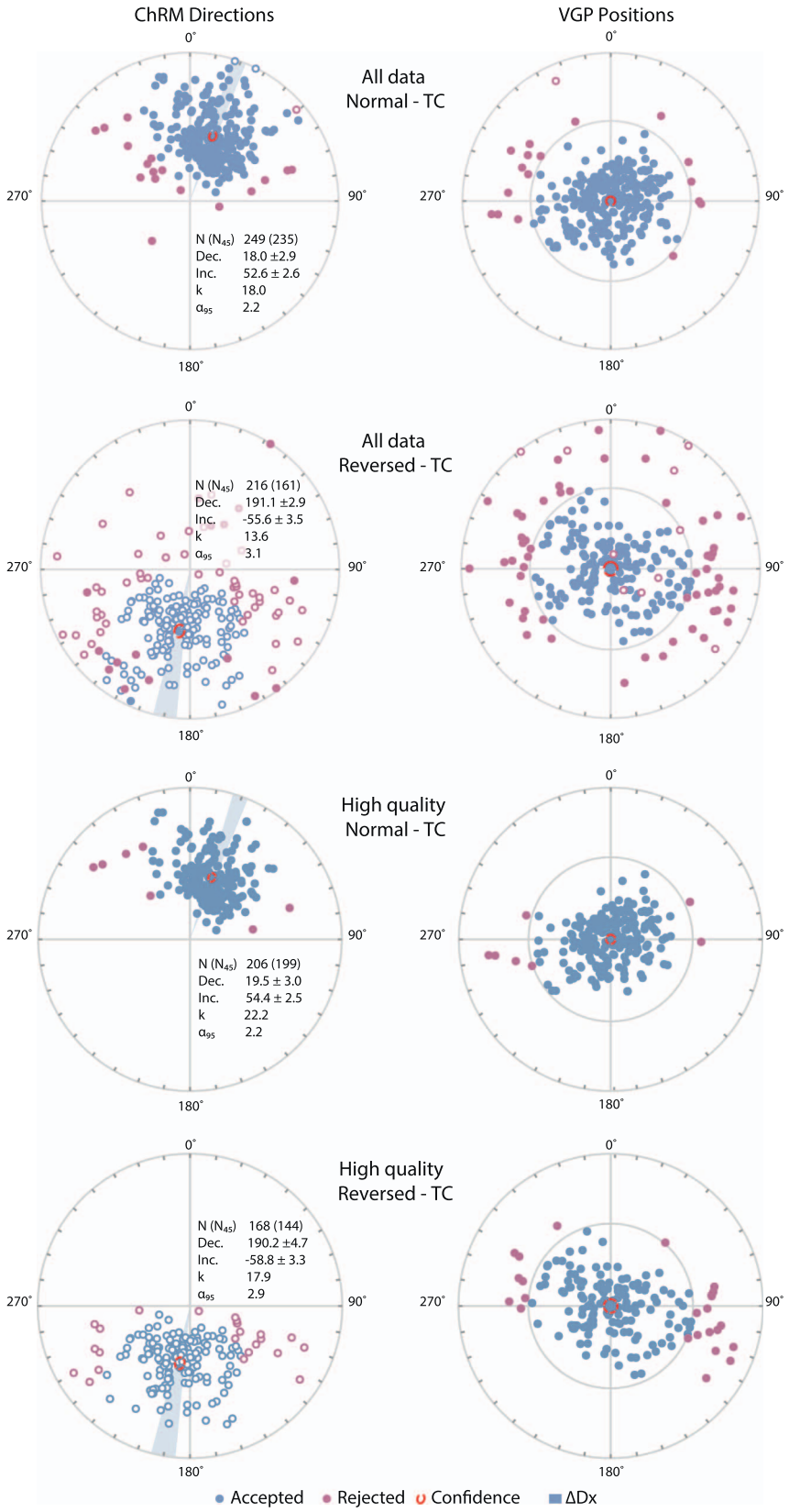

Fig. 6. Characteristic remanent magnetization directions in equal area projection. Data is grouped by interpreted polarity.

Palaeogene (Palaeocene, lower and middle Eocene) and Upper Cretaceous. In some cases, they make up the bulk of coccoliths and outnumber in-situ coccoliths, which is typical for flysch and molasse deposits. Particularly rich reworked associations were noticed in the lower (samples AMM 1.04 (at 40 m) to AMM 1.7 (at 186 m)) and in the uppermost parts of the section (samples AMM 1.20 (at 721 m) to AMM 1.34 (estimated at 1190 m; Table 1). Preservation of nannofossils varies from poor to moderate. A good preservation is observed only in sample 1.04.

In the lower part of the section (samples AMM 1.04 to AMM 1.16,

Table 1
Nannoplankton results.

Calcareous nannoplankton species	AMM 1.04	AMM 1.06	AMM 1.1	AMM 1.3	AMM 1.6	AMM 1.7	AMM 1.10	AMM 1.13	AMM 1.16	AA 01	AMM 1.20	AMM 1.23	AMM 1.30	AMM 1.34
Stratigraphic level (m) (Estimated position based on GPS)	40	(55)	63	92	124.6	186	276.1	370.2	469.2	660	721.6	806	(1184)	(1190)
Blackites spinosus (Deflandre)Blackites spinosus (Deflandre)Blackites spinosus (Deflandre)						x				x		x		
Braarudosphaera bigelowii (Gran et Braarud)Braarudosphaera bigelowii (Gran et Braarud)Braarudosphaera bigelowii (Gran et Braarud)			x	x		x	x		x					
Bramletteius serraculoides GartnerBramletteius serraculoides GartnerBramletteius serraculoides Gartner			x											
Chiasmolithus oamaruensis (Deflandre)Chiasmolithus oamaruensis (Deflandre)Chiasmolithus oamaruensis (Deflandre)									x					
Clausicoccus fenestratus (Deflandre)Clausicoccus fenestratus (Deflandre)Clausicoccus fenestratus (Deflandre)						x								
Clausicoccus vanheckiae (Perch-Nielsen)Clausicoccus vanheckiae (Perch-Nielsen)Clausicoccus vanheckiae (Perch-Nielsen)										x				
Coccolithus eopelagicus (Bramlette et Riedel)	x		x	x	x	x	x		x	x	x	x	x	
Coccolithus formosus (Kamptner)Coccolithus formosus (Kamptner)Coccolithus formosus (Kamptner)	x	x	x	x	x	x	x	x	x	x	x	x	x	x
Coccolithus pelagicus (Wallich)Coccolithus pelagicus (Wallich)Coccolithus pelagicus (Wallich)	x	x	x	x	x	x	x	x	x	x	x	x	x	x
Coccolithus subdistichus (Roth et Hay)Coccolithus subdistichus (Roth et Hay)Coccolithus subdistichus (Roth et Hay)	x		x	x					x	x		x		
Cribrocentrum reticulatum (Gartner et Smith)Cribrocentrum reticulatum (Gartner et Smith)Cribrocentrum reticulatum (Gartner et Smith)	x	x	x	x	x	x								
Cyclicargolithus floridanus (Roth et Hay)Cyclicargolithus floridanus (Roth et Hay)Cyclicargolithus floridanus (Roth et Hay)	x	x	x	x	x	x	x	x	x	x	x	x	x	x
Cyclicargolithus luminis (Sullivan)Cyclicargolithus luminis (Sullivan)Cyclicargolithus luminis (Sullivan)			x	x										
Dictyococcites bisectus (Hay, Mohler et Wade)Dictyococcites bisectus (Hay, Mohler et Wade)Dictyococcites bisectus (Hay, Mohler et Wade)	x	x	x	x	x	x	x	x	x	x	x	x	x	x
Dictyococcites stavensis (Levin et Joerger)Dictyococcites stavensis (Levin et Joerger)	x		x						x			x		
Discoaster barbadiensis TanDiscoaster barbadiensis Tan	x		x	x	x									
Discoaster deflandrei Bramlette et RiedelDiscoaster deflandrei Bramlette et Riedel	x		x			x			x					
Discoaster saipanensis Bramlette et RiedelDiscoaster saipanensis Bramlette et Riedel	x	x	x	x	x									
Discoaster tani nodifer Bramlette et RiedelDiscoaster tani nodifer Bramlette et Riedel									x					
Discoaster tanii Bramlette et RiedelDiscoaster tanii Bramlette et Riedel			x			x	x		x			x		
Helicosphaera compacta Bramlette et WilcoxonHelicosphaera compacta Bramlette et Wilcoxon						x								
Helicosphaera euphratis HaqHelicosphaera euphratis Haq						x	x		x					
Isthmolithus recurvus DeflandreIsthmolithus recurvus Deflandre	x		x		x	x	x		x	x		x		x
Lanternithus minutus StradnerLanternithus minutus Stradner	x	x	x	x	x	x	x	x	x	x		x	x	x
Pemma basquense (Martini)Pemma basquense (Martini)			x		x									
Pemma papillatum MartiniPemma papillatum Martini			x											
Pemma rotundum KlumppPemma rotundum Klumpp						x								
Pontosphaera plana (Bramlette et Sullivan)Pontosphaera plana (Bramlette et Sullivan)							x							
Pyrocyclus hermosus Roth et HayPyrocyclus hermosus Roth et Hay	x			x	x		x		x	x		x	x	

(*continued on next page*)

Table 1 (*continued*)

Calcareous nannoplankton species	AMM 1.04	AMM 1.06	AMM 1.1	AMM 1.3	AMM 1.6	AMM 1.7	AMM 1.10	AMM 1.13	AMM 1.16	AA 01	AMM 1.20	AMM 1.23	AMM 1.30	AMM 1.34
Stratigraphic level (m) (Estimated position based on GPS)	40	(55)	63	92	124.6	186	276.1	370.2	469.2	660	721.6	806	(1184)	(1190)
Reticulofenestra hillae Bukry et PercivalReticulofenestra hillae Bukry et Percival	x	x	x	x	x	x	x	x	x	x	x	x		x
Reticulofenestra minuta Roth	x	x	x	x	x	x	x	x	x	x	x	x	x	x
Reticulofenestra placomorpha (Kamptner)			x											
Reticulofenestra umbilica (Levin)	x	x	x	x	x	x	x	x	x	x	x	x	x	
Sphenolithus predistentus Bramlette et Wilcoxon										x				x
Sphenolithus pseudoradians Bramlette et Wilcoxon			x	x			x		x				x	
Transversopontis obliquipons (Deflandre)	x		x	x										
Transversopontis pulcheroides (Sullivan)			x			x		x						
Zygrhablithus bijugatus (Deflandre)	x	x	x	x	x	x	x	x	x	x	x	x	x	x
Dominated preservation state; G - good, M - moderate, B - bad	G	B	M	B	M	B	M	B	B	M	B	B	B	B
Redeposited Paleocene and Eocene	16		16	9	15	15	18	10	9	12	8	10	1	0
Redeposited Upper Cretaceous		5	13	11	13	22	14	6	11	15	10	13	10	5
Redeposited Lower and Upper Cretaceous	17					NP 21								
Position	NP 19–20													
	Eocene						Oligocene							

with two exceptions) both the diversity of nannofossil assemblages and abundance of coccoliths is higher than in the upper part. The most common species are: *Coccolithus pelagicus* (Wallich), *Cyclicargolithus floridanus* (Roth & Hay) and *Dictyococcites bisectus* (Hay, Mohler & Wade). They are accompanied by some representatives of the genus *Reticulofenestra*. Stratigraphically significant species are: *Isthmolithus recurvus* Deflandre, *Discoaster barbadiensis* Tan, *Discoaster saipanensis* Bramlette & Riedel, *Cribrocentrum reticulatum* (Gartner & Smith) and *Pemma basquense* (Martini). *Isthmolithus recurvus* has its first occurrence (FO) in the upper Priabonian and was accepted as the marker species for the base of the NP19 Zone (Hay et al., 1966; emend. Martini, 1970). The last occurrence (LO) of *D. barbadiensis* and/or *D. saipanensis* documents the upper boundary of the NP20 Zone (Hay et al., 1966). The boundary between NP19 and NP20 Zones was correlated with the FO of *Sphenolithus pseudoradians* Bramlette & Wilcoxon (Martini, 1970). *Sphenolithus pseudoradians* cannot be used as a marker species due to its similarity to the older *S. radians* Deflandre species, and a diachronous appearance in different basins (Perch-Nielsen, 1985b). The combined NP19/NP20 Zone is defined as the interval from the FO of *I. recurvus* to the LO of *D. barbadiensis/D.saipanensis* (after Aubry, 1983). The lower part of the section (from sample AMM 1.02 to AMM1.6) is in this zone.

Beginning from the sample AMM1.10 up to the top of the section, the taxonomical diversification of the assemblages gradually diminishes. The most abundant species in this part of the section are: *Coccolithus formosus* (Kamptner), *Coccolithus pelagicus* (Wallich), *Reticulofenestra hillae* Bukry & Percival, *Reticulofenestra umbilica* (Levin) as well as the small *Reticulofenestra minuta* Roth. In this part of the section only some isolated findings of poorly preserved specimens of *D. barbadiensis* or *D. saipanensis* accompanied by some Middle/Upper Eocene taxa were noticed, suggesting an allochtonous origin (redeposition). In the uppermost part of the section, a second influx of reworked Cretaceous coccolith taxa is observed. Species that are typical for NP23 (FO *Sphenolithus distentus*) and NP24 (FO *Sphenolithus ciperoensis*) are not found.

3.2.2. Coccolith limestones

Millimetres thick layers of laminated limestone were found in the Deutenhausen beds (around a stratigraphic height of 20 m). In total 20 bands were recognized, making up a total thickness of 7.7 cm, distributed over an 8.5 m interval. The thickness of individual layers varies between 0.1 and 1.75 cm (Fig. 8A). The layers are intercalated with mudstones, fine to medium grained sandstones, marls and shales. The thin limestone layers consist of an alternation of light laminae (thickness 100–600 μm) and dark laminae (thickness 50–200, rarely 700 μm). The light laminae form a so-called micronodula structure, formed by pellets packed within the light laminae. The pellets vary in size from 50 to 500 μm in length and ~30–250 μm in width, rarely up to 500 μm in width. Shapes are lenticular to oval (Fig. 8B). Composition, size and shape of pellets suggests that they could be fossil representatives of fecal pellets produced by the present-day zooplankton Copepoda (e.g. Honjo and Roman, 1978). Dark laminae are generally composed of detrital material, fine pyrite and organic matter. The light laminae are almost entirely composed of coccoliths, which are usually well preserved and often form coccospheres (Fig. 8C). Based on the SEM and supported by an optical microscope analyses, low diversity in terms of taxonomic groups is observed. The observed coccoliths are represented primarily by *Reticulofenestra minuta* Roth and *Reticulofenestra hillae* Bukry et Percival.

The textures and structures in these limestones are similar to the Oligocene thin laminated coccolith limestones (e.g. Tylawa, Jasło, Sokoliska limestones) from the Outer Carpathians (e.g. Ciurej and Haczewski, 2012, 2016). These limestones are interpreted as the intensive coccolithophore blooms, occurring seasonally (likely annually) in the Paratethyan domain (e.g. Ciurej and Haczewski, 2012 and references therein). The limestones from the Ammer section also likely represent seasonally or annually occurring coccolithophore blooms.

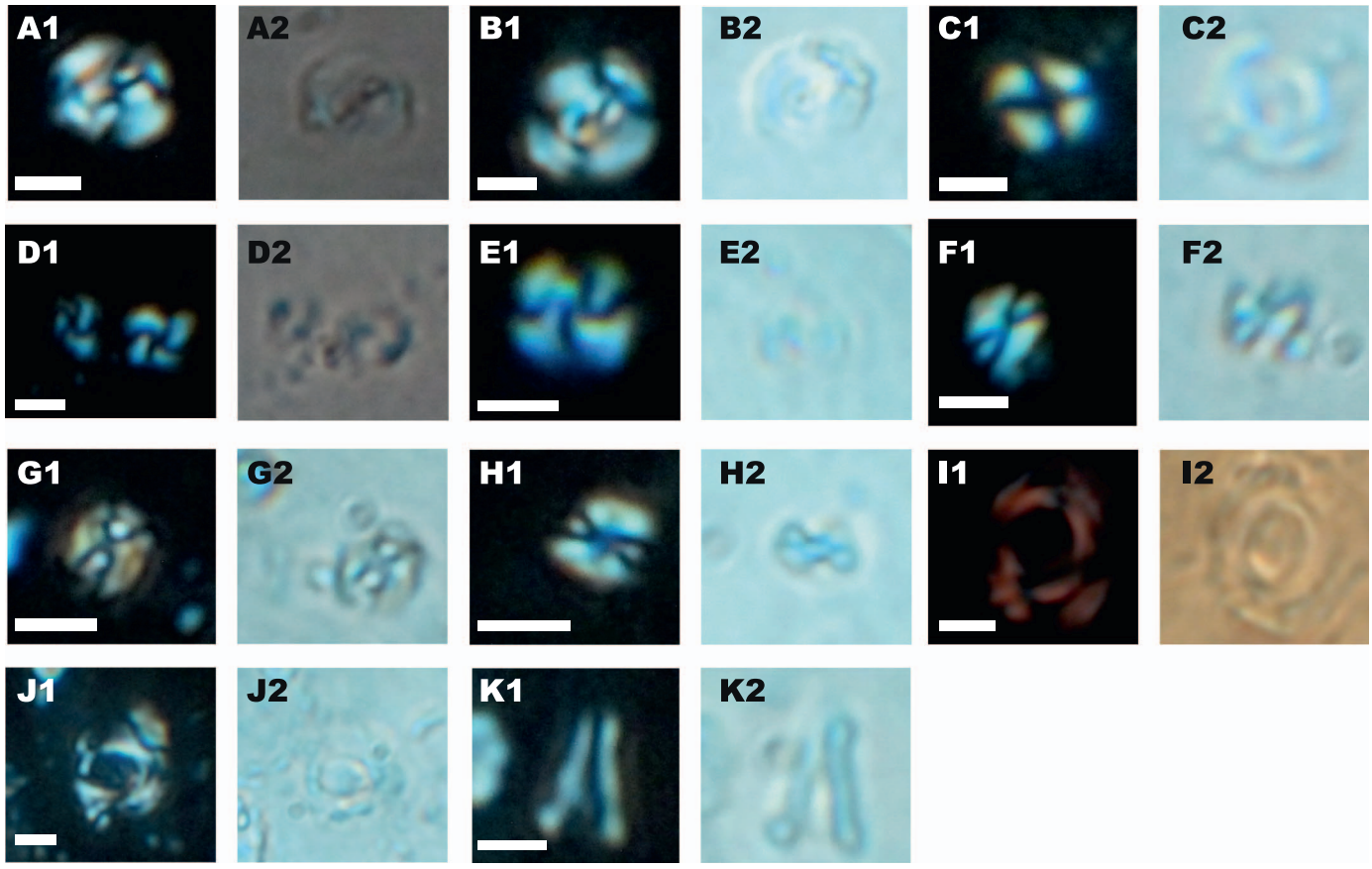

Fig. 7. Photographs of calcareous nannofossils, A1-K1, crossed nicols; A2-K2, normal light. Scale = 5 μm. A – *Dictyococcites bisectus* (Hay, Mohler et Wade), sample AMM1.23; B – *Dictyococcites bisectus* (Hay, Mohler et Wade), sample AMM1.34; C – *Coccolithus pelagicus* (Wallich) sample AMM1.23; D – *Cyclocargolithus floridanus* (Roth et Hay), sample AMM1.23; E - *Cyclocargolithus floridanus* (Roth et Hay), sample AMM1.34; F, G – *Lanternithus minutus* Stradner, sample AMM1.23; H - *Lanternithus minutus* Stradner, sample AMM1.34; I – *Reticulofenestra hillae* Bukry et Percival, sample AMM1.34; J – *Reticulofenestra umbilica* (Levin), sample AMM1.23; K – *Zygrhabilithus bijugatus* Deflandre, sample AMM1.23.

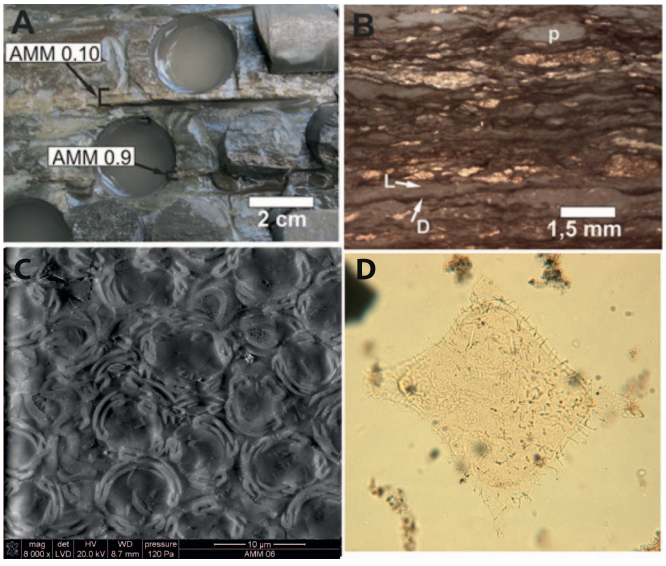

Fig. 8. A. Field view of the thin layers of laminated limestone, with the position of some samples. B. Optical microscope image showing the thick light laminae (L) composed of coccolithophores (panel C) separated by thinner dark laminae (D), composed of detrital material. The laminae are more or less laterally continuous with varying thickness, and undulated boundaries. Pelletal structures (p), composed of coccolithophores, are present in all light laminae (AMM 0.6). C. SEM images of the thin section, showing coccolithophore remains packed within pellets in the light laminae; note the numerous of intact well-preserved coccospheres (some indicated by arrows) (AMM 0.6). D. Dinoflagellate species *Wetzeliella symmetrica* in sample AM54.

Regionally extensive coccolith blooms occurred in the Paratethys in NP23, NP24 and NP25 (ca. 32 Ma–25 Ma) (e.g. Ciurej and Haczewski, 2016). The occurrence of *Reticulofenestra hillae* Bukry et Percival (ranging from NP17 to NP22) suggests that the coccolith blooms of the Ammer section are older, as the uppermost occurrence of this nannoplankton species is in NP22 (Bown and Dunkley Jones, 2012). In combination with the presence of *I. recurvus* (NP19/20–NP22) in the same interval, this limits the lower part of the section to NP19/20-NP22. This fits well with the previous study of Dohmann (1991), which places the Deutenhausen beds in NP21 or NP22.

3.2.3. Dinoflagellate cysts

For palynological purposes, we studied 19 samples from the Deutenhausen and Tonmergel beds, results of which are summarised in Table 2. Qualitative analyses were performed if preservation state allowed. In general, many of the recovered palynological assemblages yield reworked material of the Cretaceous and Palaeogene; e.g. *Apectodinium* spp. and *Dinogymnium* spp. In addition, some levels contain high amounts of amorphous organic matter. The observed dinocyst assemblages are generally not very diverse and are often dominated by a few species only.

Age control for the studied samples can be obtained by comparing our dinocyst record to the well-established dinocyst record in the Mediterranean and Atlantic region (e.g. Brinkhuis, 1994; Egger et al., 2016; Powell, 1992; Pross et al., 2010; Williams et al., 2004). Given the reworking, which is often a dominant component in molasse deposits, we favour age-assignments based on 'First Occurrences' (FO) rather than Last Occurrences (LO). Many of the well-established late Eocene–early Oligocene index taxa were not observed in the Ammer section.

Table 2
Dinoflagellate results.

Dinoflagellate cysts	AM 7.1	AM 14.3	AM 17.2	AM 18.3	AM 21.1	AM 25.3	AM 35.2	AM 36.1	AM 37.1	AM 42.3	AM 44.3	AM 45.1	AM 49	AM 51.2	AM 53.2	AM 55	AM 57.3	AM 78	AM 95.2
Stratigraphic level (m)	10.9	68.0	92.2	104.0	138.9	186.2	285.5	293.3	308.0	371.2	390.0	398.5	419.2	436.5	446.0	470.4	478.7	685.0	802.5
Achomosphaera sp.		p						p											
Apectodinium spp.											p						p		p
Areoligera spp.		p									p	p							
Areosphaeridium diktyoplokum		p				p					p			p			p		
Areosphaerdium spp.									p										p
Batiacasphaera sp.			A	A	p		p		A		A			A			p	p	
Brigantedinium spp.			p				p												
Cerodinium spp.														p					
Charlesdowniea clatrata						p													
Charlesdowniea coleothrypta subsp. *rotundata* sensu *De Coninck 1986*					p														
Charlesdowniea spp.								p		p	p					p	p		
Cordosphaeridium cantharellus												A							
Cordosphaerdium spp.							p	p							p				
Chiroptedinium sp.	?		?											?					
Cleistosphaeridium spp.						p													
Cribroperidinium tenuitabulatum					p					p				p	p				
Deflandrea spp.		p		p		p		p						p					p
Dino sp. 1												A							
Dinogymnium sp.																	p		
Diphyes spp.								p						p					
Distatodinium sp.							p					p		p	p				p
Enneadocysta pectiniformis		p	p		p					p		p		p			p		p
Enneadocysta sp.		p												p					
Gerdiocysta conopeum								p											
Glaphyrocysta exuberans																			?
Glaphyrocysta semitecta	p										p					p			
Glaphyrocysta spp.		p												p	p		p	p	
Homotryblium spp.								p									p		p
Hystrichokolpoma rigaudiae							p	p			p	p							
Hystrichokolpoma salacia											p								p
Hystrichosphaeridium spp.					p			p											
Lejeunecysta spp.				A				p				p						p	
Lentinia serrata?														p					
Lingulodinium machaerophorum			p																
Membranophoridium aspinatum	p				p			p			p								
Melitasphaeridium pseudorecurvatum													?						
Operculodinium spp.		p		p				p				p							
Operculodinium cf. *tiara*						p													p
Pentadinium spp.															?				
Phthanoperidinium spp.				p					p		p					p			
Phthanoperidinium/Senegalinium-group									p										
Protoperidinioid indet.			p				p												
Rhombodinium draco															?				p
Selenopemphix nephroides			p					p						p					
Spiniferites spp.		p	p	A		p		p						A					p
Stoveracysta sp.				p	p														
Thalassiphora spp.		p				p		p											
Wetzeliella articulata	p									p							p		
Wetzeliella symmetrica		**p**														**p**			
Wetzeliella cf. ***symmetrica***								**p**		**p**									

(*continued on next page*)

Table 2 (*continued*)

Dinoflagellate cysts	AM 7.1	AM 14.3	AM 17.2	AM 18.3	AM 21.1	AM 25.3	AM 35.2	AM 36.1	AM 37.1	AM 42.3	AM 44.3	AM 45.1	AM 49	AM 51.2	AM 53.2	AM 55	AM 57.3	AM 78	AM 95.2
Stratigraphic level (m)	10.9	68.0	92.2	104.0	138.9	186.2	285.5	293.3	308.0	371.2	390.0	398.5	419.2	436.5	446.0	470.4	478.7	685.0	802.5
Wetzeliella spp.			p	p		p				p				p					
Wetzellioid indet.						p	p												p
Reworking		+ +		+ +				+								+ +			
Acritarchs																			
Foram linings						p													
Amorphous material		+ +		+ + +			+ + +	+	+ + +		+ + +								
Other remarks							vfd					vfd					"Cooked"		

A = abundant, p = present, vfd = very few dinocysts.

Specimens and parts of *Areosphaeridium diktyoplokum* were observed, but these are likely reworked given that often only parts (viz. processes) or poorly preserved specimens were encountered. *Enneadocysta pectiniformis*, which has a stratigraphic range from ca. 36.5–29.3 Ma (Williams et al., 2004), is recorded in most levels within the Deutenhausen beds and the Tonmergel beds (Table 2). Another stratigraphically important recorded taxon, *Wetzeliella symmetrica,* is encountered at ca. 68 m (AM14.3) and 470 m (AM55) within the lower part of the Tonmergel beds. This species is generally regarded as "typical" Oligocene, more specifically it is considered to have its FO in NP22 (magnetochron C12r) (Van Simaeys et al., 2005). However, this species was recently recorded in low numbers in the uppermost Eocene (Magnetochron C13r, NP 21) of the western North Atlantic in the magnetostratigraphically calibrated record of Newfoundland, before it occurs in higher numbers during the Oligocene (Egger et al., 2016).

3.3. Bulk geochemical parameters

Geochemical data of the Deutenhausen, Tonmergel and Baustein beds are shown in Fig. 9. Carbonate contents range from 27 to 67 wt%. Within the Deutenhausen beds carbonate content increases upwards from 27 to 50 wt%. The average carbonate content in the Tonmergel beds is around 40 wt%. A significant increase in carbonate is observed between 888 and 925 m, in the top of the Tonmergel beds. In general, organic matter contents are low in the entire succession. The average TOC content in the Deutenhausen and Tonmergel beds is 0.3 and 0.5 wt %, respectively. A single sample near the base of the Tonmergel beds (at 308 m) contains > 1.0 wt% TOC. The hydrogen Index (HI) classifies the organic matter as kerogen type III (or IV). Only the organic matter rich sample contains organic matter with a moderately high HI (~250 mgHC/gTOC) indicating a mixture of prevailing kerogen type III with type II.

TOC/S ratios exceed 2.8, which is considered typical for brackish and non-marine sediments (Berner, 1984). This corresponds well with previous studies on the Deutenhausen beds and Tonmergel that report brackish conditions from time to time (Diem, 1986; Dohmann, 1991; Maurer et al., 2002). Apart from some single samples, intervals with TOC/S ratios below 2.8, considered as indicative for anoxic environments, prevail only in the lower (275–430 m) and middle part of the Tonmergel beds (660–695 m). However, as both, TOC and sulphur contents are low, the significance of TOC/S ratios should not be overestimated. Moreover TOC/S ratios may be increased in the presence of refractory type III(to IV) kerogen. Nevertheless, the clear trend between 660 and 790 m with TOC/S ratios increasing upwards from 1 to 30, which is a result of strongly decreasing sulphur contents and indicates increasing sulphur limitation.

Measured Tmax values range between 420 and 434 °C (average 426 °C) indicating that the thermal overprint is mild and that, therefore, the organic matter is thermally immature (Espitalié et al., 1977). No depth trend is visible in the studied succession, which is > 1000 m thick. The low maturity is also supported by vitrinite reflectance values (~0.4%Rr) measured on drift wood in the lower part of the Weißach beds (Stauner et al., 2015).

4. Discussion

4.1. Palaeomagnetism

The palaeomagnetic results show a clear magnetostratigraphic pattern with three polarity zones (R-N-R). Although several single levels show an opposite polarity, we do not consider these representative of short magnetozones. Our magnetostratigraphy does not show enough reversals to correlate to the geomagnetic polarity time scale based solely on matching polarity patterns. We therefore require additional age constraints, in casu the biostratigraphy.

The mean of the high quality reversed directions (D = 10.2° ± 3.0,

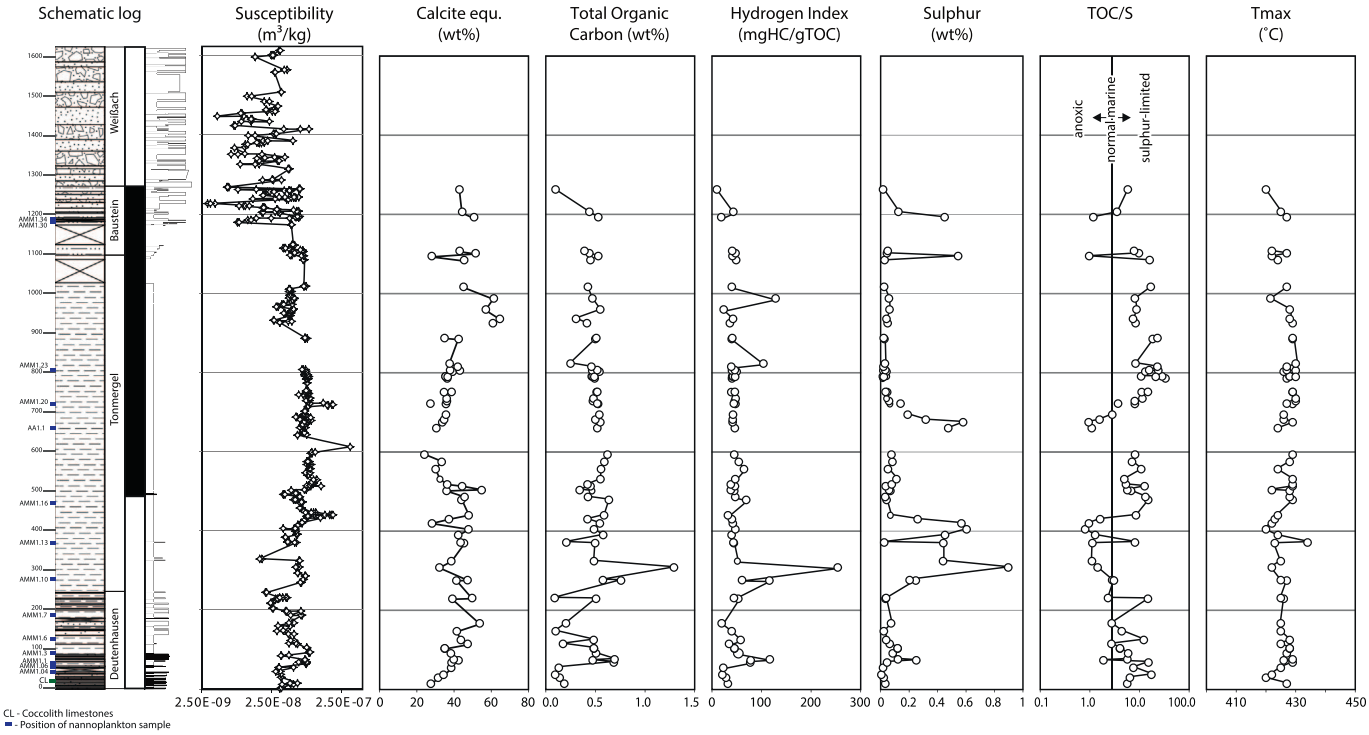

Fig. 9. Log of the section with bulk magnetic susceptibility and bulk geochemical data.

I = 58.8° ± 3.3) is within error of the expected directions (D ≈ 7.5° ± 3.5, I ≈ 60.8° ± 2.5) for the Eurasian plate at 34 Ma (GAPWaP; Torsvik et al., 2012). The mean of the high quality normal directions (D = 19.5° ± 3.0, I = 54.4° ± 2.5) shows a significantly shallower inclination than predicted by the GAPWaP, while the declination shows a clockwise deviation of > 10°. The difference between the normal and reversed directions might be caused by the fact that the reversed polarities are mostly recorded in the coarser lithologies of the Deutenhausen and Weißach beds and implies that these lithologies do not show shallowing of the inclination due to compaction. The shallow normal inclinations are recorded mostly in the Tonmergel beds, suggesting that the Tonmergel beds was affected by compaction. If we apply the E/I inclination shallowing correction (Tauxe and Kent, 2004) the mean normal inclination does not become significantly steeper (55.6° with a 95% confidence interval ranging 54–64°). Possibly, the difference between normal and reversed directions may partially result from an unremoved normal overprint which is more difficult to recognise in normal polarity samples, and partially from differences in lithology.

Although the normal and reversed distributions have a negative reversal test, combining both datasets could average out the unremoved component. The combined dataset has a mean declination of 16.7° ± 2.6. This implies a clockwise rotation of ~10°, with respect to the expected Eocene direction. This declination is also found in studies from the Swiss part of the NAFB, which reports declinations of 16–17° (Kempf et al., 1998). We hesitate however to conclude that the NAFB has rotated with respect to Eurasia, considering the fact that the reversed directions are within error identical to the expected Eocene direction, and may more reliably have recorded the geomagnetic field direction.

4.2. Biostratigraphy

4.2.1. Nannoplankton zonation

According to the standard nannoplankton zonation of Martini (1970), the top of NP20 corresponds to the Eocene-Oligocene (E-O) boundary. The lower part of NP21 was included into the Oligocene, based on the study of the Priabonian stratotype section (Verhallen and Romein, 1983). The E-O boundary stratotype is defined in the Massignano section near Ancona, Italy (Premoli Silva and Jenkins, 1993), with the boundary placed on the extinction of planktonic foraminifer genera *Hantkenina* and *Cribrohantkenina*. The calcareous nannofossil zones NP21 of Martini (1971) and CP16a of Okada and Bukry (1980) contain the E-O boundary in the Italian sections (Coccioni et al., 1988). Within the North Sea basin, the E-O boundary in NP21 is further specified by the LO of *Pemma basquense* (Martini) and/or *Pemma papillatum* Martini (Varol, 1999), although these species are rare, which impedes correlation to other basins. Only few specimens as well as some isolated plates belonging to the genus *Pemma* were observed in samples AMM1.1 and AMM1.3. In sample AMM1.7 only *Pemma rotundum* Klumpp was identified, which is known from upper Eocene deposits in Germany (Varol, 1999). *Cribrocentrum reticulatum* (Gartner & Smith) has its LO in the lower part of NP21, just below the LO of *Pemma basquense/Pemma papilatum*. Within the studied section abundant and continuous representation of *C. reticulatum* was observed from the base of the section up until sample AMM1.7. Above this level, only few slightly damaged specimens are found, which are likely reworked. *Lanternithus minutus* Stradner was common in sample AMM1.10. Abundant presence of *L. minutus* in the lowermost Oligocene was reported in the North Sea Basin (Varol, 1999). Also “cold water” species *I. recurvus* is more abundant in sample AMM1.16 which could reflect a decrease of surface water temperature caused by the climatic cooling around the Eocene-Oligocene transition. Thus, the upper part of the section is supposed to represent the lowermost Oligocene (Lower Rupelian, previously Latdorfian). It corresponds to zone NP21 because of the occurrence of *C. formosus*. The LO of this species indicates the upper boundary of NP21 (Martini, 1970; Perch-Nielsen, 1985b; Varol, 1999). Based on nannoplankton biostratigraphy, we conclude that the *E*-O boundary is located between sample AMM1.7 and AMM1.10 (186–276.1 m).

4.3. Magneto-biostratigraphic time frame for the Ammer section

The sampled part of the Ammer section consists of three polarity

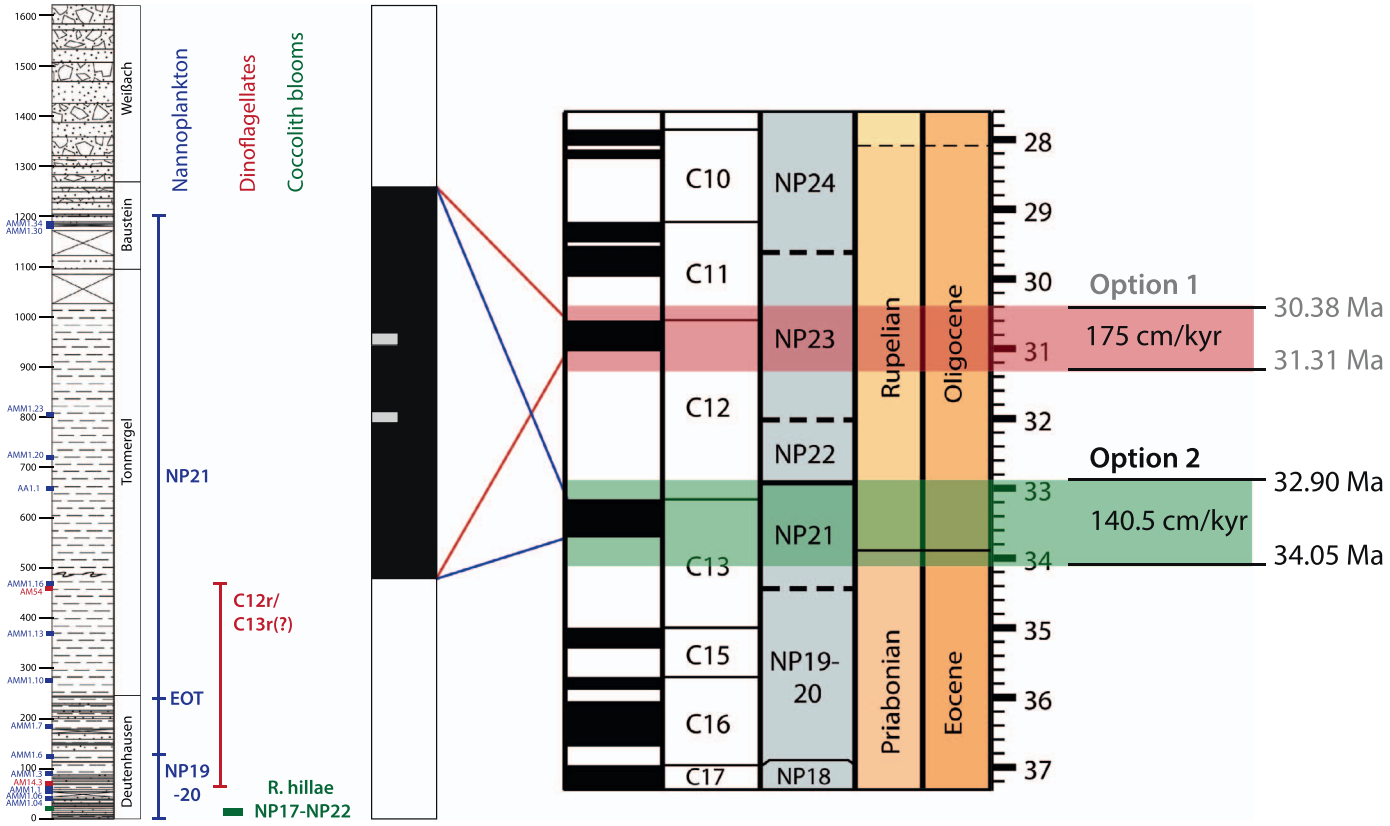

Fig. 10. Possible correlations of the Ammer section to the geologic time scale (TSCreator), with calculated sediment accumulation rates and resulting ages for the lower and upper boundaries of the section.

zones, starting with a reversed polarity interval from the bottom of the section up to 490 m (Fig. 6). Then there is a normal polarity interval of 770 m, from 490 up to 1260 m. The top part of the section shows a reversed polarity again up to the top at 1620 m. The observed nannoplankton assemblages and coccolith blooms limit the section to the time interval from NP19/20 (FO of *Isthmolithus recurvus*) to NP22 (LO of *Reticulofenestra hillae* Bukry et Percival, which occurs in blooms in the Deutenhausen beds). Traditionally, dinoflagellate cyst *Wetzeliella symmetrica* occurs from NP22 (e.g. Van Simaeys et al., 2005). As these nannofossil and dinocyst constraints are not compatible, we discuss two options (Fig. 10) for correlation of the Ammer section to the Geologic Time Scale (Gradstein et al., 2012). We correlate the section based on the magnetostratigraphic pattern and the biostratigraphic constraints, realizing that the boundary between nannoplankton zones NP19–20 and NP21, as well as the boundary between NP22 and NP23, is not firmly defined. Hiatuses are likely present in the Weißach beds, but since we have not observed major hiatuses in the Deutenhausen, Tonmergel and Baustein units, we assume that we have sampled a continuous succession.

4.3.1. Option 1

Considering the FO of *Wetzeliella symmetrica* to occur in magnetochron C12r implies that the normal polarity interval of the Ammer section corresponds to C12n. This correlation furthermore indicates that the entire UMM in the Ammer section is positioned in NP23, while this nannofossil zone has not been observed in the entire western NAFB. The blooms of the coccolithophore *Reticulofenestra hillae* Bukry et Percival at 20 m in the Deutenhausen beds are then positioned either in the top of NP 21 or in NP22 (thus older than ~32 Ma; see Fig. 10). Consequently, the sediment accumulation rate for the lower (reversed) part of the Tonmergel succession must be much (~6 times) lower (~250 m in ~1 Myr) than for the upper (normal) part (~500 m in 300 kyr). As the lower part of the section shows a shallowing from the turbiditic sands of the Deutenhausen beds to shelf deposits of the Tonmergel beds, this seems unlikely. Alternatively, the position of the NP22–23 boundary is incorrect in the GTS and should be placed at a much younger level. Another possibility is that there are gaps in the stratigraphic record of the Ammer section, for which we find no indications. Assuming constant sediment accumulation rates for the normal polarity zone in the Ammer section, we interpolate the ages of the minimum and maximum ages of the section. The duration of C12n is 440 kyr (Gradstein et al., 2012), leading to a sediment accumulation rate of 175 cm/kyr. Extrapolating this sediment accumulation rate, the bottom of the section then ends up at an age of 31.31 Ma, and the top at 30.38 Ma (see Fig. 10).

4.3.2. Option 2

Nannoplankton assemblages indicate that the section corresponds to NP19/20-NP21. The only normal polarity interval from the top of NP19/20 to NP21 is C13n. In this case, the finding of *W. symmetrica* within the magnetochron C13r is older than its generally assumed FO, but might correspond to the observation of some specimens in Chron C13r in the north-Atlantic that are grouped as "*W. symmetrica-W. gochtii*" (Egger et al., 2016). The duration of C13n is 548 kyr (Gradstein et al., 2012), which leads to an average sediment accumulation rate of 140.5 cm/kyr. Extrapolation of this rate gives ages for the bottom of the section of 34.05 Ma and the top of 32.90 Ma.

We prefer option 2 for the correlation, since this agrees with the observed nannoplankton assemblages, other reported nannoplankton and foraminiferal assemblages from the Deutenhausen and Tonmergel beds (Dohmann, 1991) and the observation of *Wetzeliella symmetrica* in C13r (latest Eocene) as reported by Egger et al. (2016). Furthermore, no nannoplankton assemblages that are typical for NP23 were found in the Ammer section, consistent with the absence of NP23 markers in all

other sections of the Deutenhausen and Tonmergel beds (Dohmann, 1991). The study of Dohmann (1991) shows results of biostratigraphic analyses of 53 sections of Deutenhausen, Fischschiefer and equivalent sediments (Supplementary information, Table S2). Nannoplankton analyses are often complicated by reworking and poor preservation, as is also the case for our nannoplankton biostratigraphy in the Ammer. However, Dohmann (1991) also performs biostratigraphy on planktonic foraminifera, which show good preservation in the Galon graben, near Ampfing and near Hohenlinden. In these sections and cores, the Eocene-Oligocene transition is pinpointed using foraminifera. In most sections, nannoplankton assemblages yield ages from NP19/20 to NP22. In only three sections, an age of NP23 is inferred, of which two are based on a complete absence of nannoplankton and not on findings of biostratigraphic markers for NP23. Biostratigraphy of the Ammer section results in an age of NP21/NP22 for the Deutenhausen beds (Dohmann, 1991). As no distinction could be made between NP21 and NP22 in the study of Dohmann (1991), his interpretation fits with our nannoplankton findings of NP19/20-NP21.

Assuming a constant sediment accumulation rate and using the palaeomagnetic reversals as tie-points, we estimated the ages of lithological transitions in the Ammer section. This results in an age of 33.88 Ma for the Deutenhausen-Tonmergel boundary and 33.27 Ma for the Tonmergel-Baustein boundary. The marine-continental transition at the Baustein – Weißach boundary occurred at 33.15 Ma. Assuming constant sediment accumulation rates for the Tonmergel succession is reasonable as there are no significant changes in lithology. However, we also realize that the major change to Baustein beds may be accompanied to changes in accumulation rates. Taking the other extreme, that there is “no time” in the Baustein deposition, the calculated age for the marine continental transition remains around the age of 33.15 Ma, as this transition is dated by the top of chron C13n (Fig. 10). The coccolith blooms of *R. hillae* within the Deutenhausen beds in the Ammer section are then late Eocene in age, which is older than the coccolith blooms in the top of the Schöneck Formation (NP22; Schulz et al., 2005).

Fig. 11 shows our preferred correlation of the Ammer section to the Geologic Time Scale (Gradstein et al., 2012), with the oxygen isotope record of Coxall et al. (2005). The Eocene-Oligocene transition is characterised by two pronounced sea-level drops (Houben et al., 2012). The oldest of these (the EOT-1 event) is interpreted as a sea-level drop of around 20 m, and occurs just below the Eocene-Oligocene boundary in C13r. The Tonmergel-Deutenhausen transition effectively corresponds to the Eocene-Oligocene boundary, so this sea-level drop could have caused a transition from the slope facies of the Deutenhausen beds to the shallower shelf facies of the Tonmergel beds (see Fig. 2). The younger sea-level drop, Oi-1, is larger, an estimated 50–60 m (Houben et al., 2012), but this event occurs in the bottom of C13n, which corresponds to a stratigraphic height of around 490 m in the Ammer section. Although no major sedimentological changes are observed, there is a conspicuous sand lens around this level, which shows intense slumping in the otherwise homogeneous Tonmergel beds (see detailed log, Fig. S1, Supplementary information).

4.4. Ammer section in Paratethys context

During the middle to late Eocene, the peri-Tethys region was already sensitive to periodical restriction, characterised by dysoxic to anoxic deposits (e.g. Beniamovski et al., 2003). After the Paratethys formed in the early Oligocene, this basin recorded oxygen-poor conditions until the middle Miocene, leading to deposition of black shales in the Eastern Paratethys for millions of years (e.g. Popov et al., 2008). The Paratethys had brackish episodes, with endemic fauna (e.g. Popov and Studencka, 2015; Vasiliev et al., 2004; Wessely, 1987), indicating a severe restriction from the global ocean.

The Deutenhausen and Tonmergel beds in the Ammer section are argued to be time-equivalents of the fish shales of the Schöneck Formation, deposited in deeper parts of the NAFB (Dohmann, 1991). Schulz et al. (2002) subdivided the Schöneck Formation into a marly

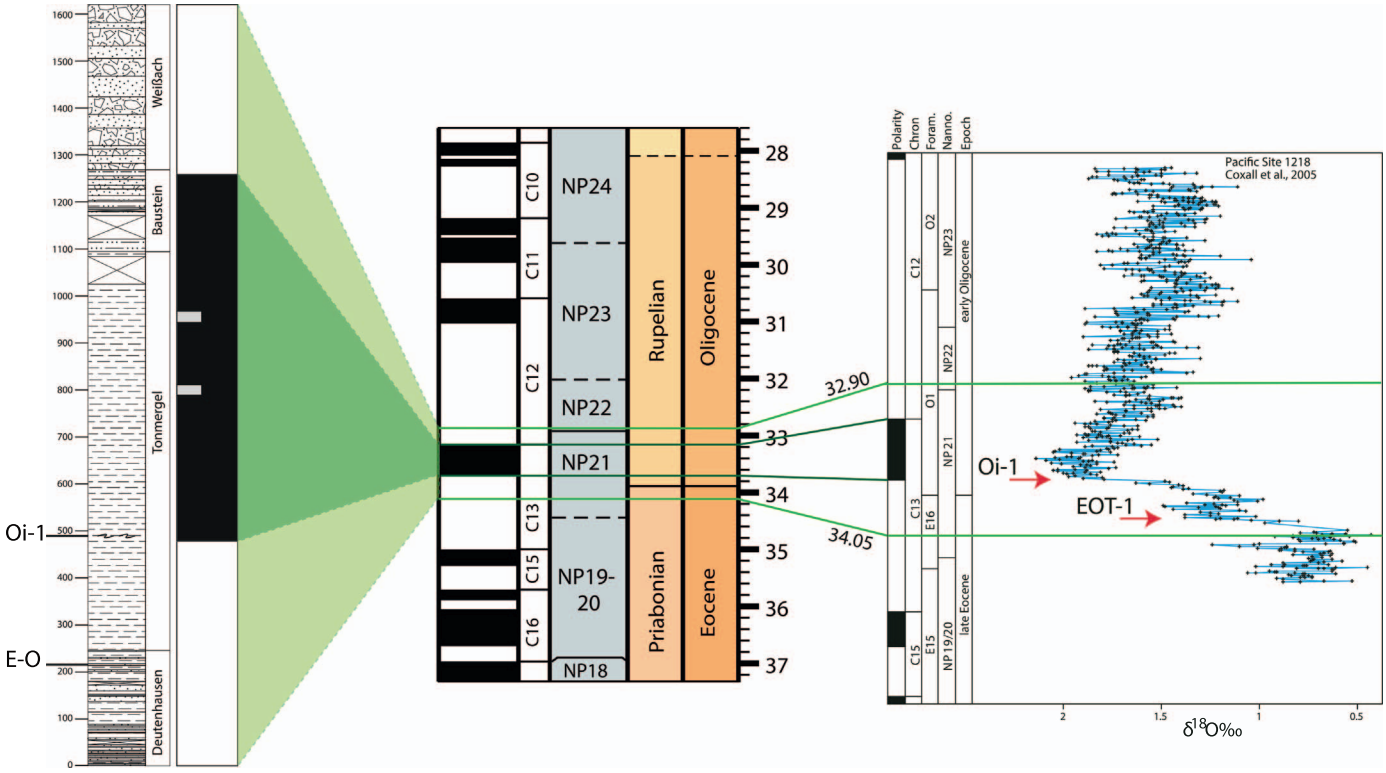

Fig. 11. Correlation of the Ammer section to the geologic time scale (TSCreator), and the sea-level curve around the Eocene-Oligocene transition of Coxall et al., 2005. (Modified after Miller et al., 2009.)

lower part (their units "a/b"; ~10 m thick), and a shaly upper part (their unit "c"), which typically attains a thickness of a few metres. Comparing the Schöneck and Tonmergel beds, differences in thickness and organic matter richness are most striking. The huge thickness of the Tonmergel beds reflects its proximal depositional environment and high detrital influx from the southern margin of the NAFB. The low TOC content of the Tonmergel beds (average 0.5 wt%) compared to that in units "a/b" of the Schöneck Formation (average 2.2 wt%) may be the combined effect of organic matter dilution by detrital material and the shallow depositional environment, which impaired organic matter preservation.

According to Schulz et al. (2002), units "a/b" represent nannoplankton zones NP19–20 to NP21. Since diagnostic nannoplankton species are missing in the carbonate-free rocks of unit "c", no zonation could be established, although the top of NP21, or NP22 is estimated for the lower part of this unit. The lack of detailed time constraints inhibits a direct correlation of the Schöneck Formation to the Ammer section.

Nonetheless, we hypothesize that the marine-continental transition in the Ammer section coincides with the boundary between units "a/b" and "c". This boundary represents a change from dysoxic to anoxic conditions (Schulz et al., 2002), suggesting that the cut-off of the NAFB gateway as documented in the Ammer section has profound implications for the rest of the basin.

Our new results from the Ammer section show that in the NAFB a shallowing of the connection of the Paratethys to the open ocean occurred around the EOT. We date the final closure of this gateway (at the Baustein-Weißach boundary) at 33.15 Ma. This fundamentally improves our understanding of the timing of restriction of the Paratethys, since the NAFB was one of its few gateways.

Reichenbacher et al. (2004) report an age for the marine-continental transition around the Rupelian-Chattian boundary (~28 Ma), based on otolith and charophyte zonations of the Cyrena beds (transitional, brackish facies between the UMM and USM) that overlie the Baustein beds. Kempf and Pross (2005) have studied the transition of the UMM to USM in the Wilhelmine Alpe section, which is almost 70 km west of the Ammer section, and correlate their results to several studies in the Swiss part of the NAFB. The Wilhelmine Alpe section consists of ~50 m of Deutenhausen beds and ~175 m of Tonmergel beds, which is significantly less than the 850 m of Tonmergel along the Ammer river. The study of Kempf and Pross (2005) finds the transition from Tonmergel to Baustein beds in a reversed interval, which they correlate to C12r, at an age of ~31 Ma, while the transition to normal polarity takes place in the middle of the Baustein beds. Contrarily, in the Ammer section, the lower part of the Baustein beds is in a normal polarity interval. The top of the Baustein shows a transition to reversed polarities, indicating that the Baustein beds are diachronous throughout the NAFB.

The palaeomagnetic correlation of the Wilhelmine Alpe section to C12 by Kempf and Pross (2005) is mostly based on the occurrence of the dinocysts *Areoligera semicirculata*, *Wetzeliella symmetrica* and *Wetzeliella gochtii*, which are regarded as typical Oligocene taxa. A recent study by Egger et al. (2016), however, reported the presence of *W. symmetrica* and *W. gochtii* already in C13r, which matches our results of the Ammer section if we follow the age-constraints provided by the nannoplankton. The older occurrence of *W. symmetrica* and *W. gochttii* allows for an alternative correlation of the magnetostratigraphy of the Wilhelmine Alpe section to the C13r-C13n reversal at 33.7 Ma. This alternative correlation is ~2 million years older than the currently accepted age, but is somewhat closer to the Baustein-Weißach transition in the Ammer section at 33.27 Ma.

Since the Tonmergel beds are very thick in the Ammer section, the accommodation space must have been large and fairly equal to the input of sediments, to sustain deposition of 850 m of monotonous clayey marls. Sediment accumulation rates are very high when compared to the Wilhelmine Alpe section (140.5 cm/kyr for the Ammer section versus 8.6 cm/kyr for the Wilhelmine Alpe section). Creation of accommodation space was recently linked to rollback of a slab underneath the Alps (Schlunegger and Kissling, 2015). The sedimentation rate of 140.5 cm/kyr that results when choosing option 2 is rather high, but not unheard of. High sedimentation rates frequently occur in basins that are located near rising mountains, for example in the South Caspian basin, where sedimentation rates reach 130–140 cm/kyr (Lerche et al., 1997; Nadirov et al., 1997; Tagiyev et al., 1997). In addition, the Ammer sediments are interpreted as the transition from flysch to molasse for which similar (or even higher) sedimentation rates are to be expected. An example is the Karamanmaraş basin in Turkey (Hüsing et al., 2009). Turbiditic sediments in Corfu have sedimentation rates of > 125 cm/kyr (van Hinsbergen, 2004), comparable to ours and in the Carpathian foredeep sedimentation rates of up to 150 cm/kyr have been estimated (Vasiliev et al., 2004).

Because the Tonmergel is thickest in the Ammer section, we argue that the marine-continental transition would have occurred latest there. More proximal settings, which contain less Tonmergel, would see an earlier transition to continental conditions. A pre-32 Ma transition to continental deposits agrees with the absence of nannoplankton of zone NP23 in most parts of the NAFB (Dohmann, 1991). Furthermore, Sachsenhofer et al. (2017) suggest that the Polbian bed (early NP23) in the Belaya River section in Russia represents a Paratethys-wide brackish event, caused by a temporary isolation from the open ocean.

However, the Swiss sections to which Kempf and Pross (2005) correlate the Wilhelmine Alpe section show a marine-continental transition that is a few million years younger than in the Ammer section. We hypothesize that these sections retained a connection to the Mediterranean through the Rhône graben, or to the North Sea through the Upper Rhine Graben, while the connection to the Paratethys through the NAFB was closed at 33.15 Ma.

In summary, our results provide an older age for the marine-continental transition in the NAFB than previously suggested. Our new age precludes a link to a major regression around the Rupelian-Chattian boundary as earlier suggested (e.g. Andeweg and Cloetingh, 1998; Doppler et al., 2005; Lemcke, 1983; Reichenbacher et al., 2004) Hence, this transition seems not so much bound to a major eustatic sea-level change, but rather to a different mechanism, like erosion and basin infill through tectonic processes, for example as suggested by Schlunegger et al. (2007). Since foreland basin sedimentation is synorogenic, changes in tectonic processes and associated variations in the supply of sediment to the basin have a major impact on regression and transgression cycles, particularly for the central section of the Molasse basin (see summary by Schlunegger and Castelltort, 2016).

5. Conclusions

An exceptionally long section of the Lower Marine Molasse to the Lower Freshwater Molasse is exposed along the Ammer river in southern Germany. We dated this transition using magnetostratigraphy combined with biostratigraphy of nannoplankton and dinoflagellate cysts. We correlate the normal polarity interval in the section to C13n, and use this correlation to calculate sediment accumulation rates, which we subsequently use to estimate ages for lithological transitions in the section.

The transition from the Deutenhausen beds to Tonmergel beds (33.88 Ma) essentially coincides with the Eocene-Oligocene boundary (33.9 Ma). The large eustatic Oi-1 sea-level drop is not related to any major facies shift in our section, although at this level we find an intensely slumped sand layer in the otherwise homogeneous clayey marls of the Tonmergel. A shift to the shallower, coastal facies of the Baustein beds is observed (33.27 Ma). The establishment of continental conditions in this basin is represented by red conglomerates of the Weißach beds, and reflects closure of this gateway of the Paratethys Sea at 33.15 Ma. Our older age for the marine-continental transition precludes a link to a eustatic sea-level drop at the Rupelian-Chattian boundary. The closure of this NAFB connection to the open ocean promoted a long

period of dominantly oxygen-poor conditions in the Eastern Paratethys, facilitating the deposition of organic-rich shales.

We provide a detailed log (10 cm scale) with all sampled levels, Fig. S1. All interpreted directions of palaeomagnetic samples can be viewed in the web portal http://paleomagnetism.org/ through import of the Directions.dir file in the interpretation portal. Interpreted vectors are also supplied in Table S1. Statistical data can be viewed through import of the Ammer.pmag file in the statistics portal. Results of the study of Dohmann (1991) are given in Table S2. Supplementary data associated with this article can be found in the online version, at https://doi.org/10.1016/j.gloplacha.2017.12.009.

We provide a detailed log (10 cm scale) with all sampled levels, Fig. S1. All interpreted directions of palaeomagnetic samples can be viewed in the web portal http://paleomagnetism.org/ through import of the Directions.dir file in the interpretation portal. Interpreted vectors are also supplied in Table S1. Statistical data can be viewed through import of the Ammer.pmag file in the statistics portal. Results of the study of Dohmann (1991) are given in Table S2. Supplementary data associated with this article can be found in the online version, at https://doi.org/10.1016/j.gloplacha.2017.12.009.

Acknowledgements

This work was financially supported by the Netherlands Organization for Scientific Research (NWO) [grant 865.10.011] of WK. We thank Dirk van Haeringen for his contributions in the field and for palaeomagnetic analyses. The study of nannoplankton was financed by the National Science Centre (NCN) of Poland [grant 2011/01/D/ST10/04617]. We thank Bettina Reichenbacher, Uwe Kirscher, Fritz Schlunegger and one anonymous reviewer for comments.

References

Akhmet'ev, M.A., 2011. Problems of Paleogene stratigraphy and paleogeography in the middle latitudes of Eurasia. Russ. Geol. Geophys. 52, 1075–1091.
Akhmetiev, M.A., Beniamovski, V.N., 2009. Paleogene floral assemblages around epicontinental seas and straits in Northern Central Eurasia: proxies for climatic and paleogeographic evolution. Geol. Acta 7, 297–309.
Andeweg, B., Cloetingh, S., 1998. Flexure and “unflexure” of the North Alpine German-Austrian Molasse Basin: constraints from forward tectonic modelling. Geol. Soc. Lond. Spec. Publ. 134, 403–422.
Aubry, M.-P., 1983. Biostratigraphie du Paléogène épicontinentalde l'Europe du Nord-Ouest. In: Étude Fondée sur les Nannofossiles Calcaires. Doc. des Lab. géologie Lyon. 89. pp. 1–317.
Beniamovski, V.N., Alekseev, A.S., Ovechkina, M.N., Oberhänsli, H., 2003. Middle to upper Eocene dysoxic-anoxic Kuma Formation (northeast Peri-Tethys): biostratigraphy and paleoenvironments. Geol. Soc. Am. Spec. Pap. 369, 95–112.
Beniest, A., Brun, J.P., Gorini, C., Crombez, V., Deschamps, R., Hamon, Y., Smit, J., 2016. Interaction between trench retreat and Anatolian escape as recorded by neogene basins in the northern Aegean Sea. Mar. Pet. Geol. 77, 30–42.
Berger, J.-P., Reichenbacher, B., Becker, D., Grimm, M., Grimm, K., Picot, L., Storni, A., Pirkenseer, C., Derer, C., Schaefer, A., 2005a. Paleogeography of the Upper Rhine Graben (URG) and the Swiss Molasse Basin (SMB) from Eocene to Pliocene. Int. J. Earth Sci. 94, 697–710.
Berger, J.-P., Reichenbacher, B., Becker, D., Grimm, M., Grimm, K., Picot, L., Storni, A., Pirkenseer, C., Schaefer, A., 2005b. Eocene-Pliocene time scale and stratigraphy of the Upper Rhine Graben (URG) and the Swiss Molasse Basin (SMB). Int. J. Earth Sci. 94, 711–731.
Berner, R.A., 1984. Sedimentary pyrite formation: an update. Geochim. Cosmochim. Acta 48, 605–615.
van der Boon, A., Kuiper, K.F., Villa, G., Renema, W., Meijers, M.J.M., Langereis, C.G., Aliyeva, E., Krijgsman, W., 2015. Onset of Maikop sedimentation and cessation of Eocene arc volcanism in the Talysh Mountains, Azerbaijan. Geol. Soc. Lond. Spec. Publ. 428.
Bosboom, R., Dupont-Nivet, G., Grothe, A., Brinkhuis, H., Villa, G., Mandic, O., Stoica, M., Kouwenhoven, T., Huang, W., Yang, W., Guo, Z., 2014. Timing, cause and impact of the late Eocene stepwise sea retreat from the Tarim Basin (west China). Palaeogeogr. Palaeoclimatol. Palaeoecol. 403, 101–118.
Bown, P.R., Dunkley Jones, T., 2012. Calcareous nannofossils from the Paleogene equatorial Pacific (IODP Expedition 320 Sites U1331-1334). J. Nannoplankton Res. 32, 3–51.
Bown, P.R., Young, J.R., 1998. Techniques. In: Calcareous Nannofossil Biostratigraphy. Chapman and Hall, London, pp. 16–28.
Brinkhuis, H., 1994. Late Eocene to Early Oligocene dinoflagellate cysts from the Priabonian type-area (Northeast Italy): biostratigraphy and paleoenvironmental interpretation. Palaeogeogr. Palaeoclimatol. Palaeoecol. 107, 121–163.
Brinkhuis, H., Munsterman, D.K.K., Sengers, S., Sluijs, A., Warnaar, J., Williams, G.L.L., 2003. Late Eocene-Quaternary dinoflagellate cysts from ODP site 1168, off Western Tasmania. Proc. Ocean Drill. Prog. Sci. Results 189, 1–36.
Ciurej, A., 2010. Procedures for obtaining optimal SEM images of coccolithophore debris in coccolith limestones. Acta Palaeontol. Pol. 55, 169–171.
Ciurej, A., Haczewski, G., 2012. The Tylawa Limestones – a regional marker horizon in the Lower Oligocene of the Paratethys: diagnostic characteristics from the type area. Geol. Q. 56, 833–844.
Ciurej, A., Haczewski, G., 2016. The sokoliska limestone, a new regional marker horizon of coccolith laminites in the Oligocene of the outer carpathians: diagnostic features and stratigraphic position. Ann. Soc. Geol. Pol. 86, 415–427.
Coccioni, R., Monaco, P., Monechi, S., Nocci, M., Parisi, G., 1988. Biostratigraphy of the Eocene-Oligocene boundary at Massignano (Ancona, Italy). In: Premoli Silva, I. (Ed.), The Eocene–Oligocene Boundary in the Marche-Umbria Basin (Italy): Ancona, Italy. International Union of Geological Sciences, Commission on Stratigraphy, pp. 59–80.
Cowgill, E., Forte, A.M., Niemi, N., Avdeev, B., Tye, A., Trexler, C., Javakhishvili, Z., Elashvili, M., Godoladze, T., 2016. Relict basin closure and crustal shortening budgets during continental collision: an example from Caucasus sediment provenance. Tectonics 2918–2947.
Coxall, H.K., Wilson, P.A., Palike, H., Lear, C.H., Backman, J., 2005. Rapid stepwise onset of Antarctic glaciation and deeper calcite compensation in the Pacific Ocean. Nature 433, 53–57.
Da Silva, A.-C., Dekkers, M.J., Mabille, C., Boulvain, F., 2012. Magnetic susceptibility and its relationship with paleoenvironments, diagenesis and remagnetization: examples from the Devonian carbonates of Belgium. Stud. Geophys. Geod. 56, 677–704.
Dankers, P.H.M., Zijderveld, J.D.A., 1981. Alternating field demagnetization of rocks and the problem of gyromagnetic remanence. Earth Planet. Sci. Lett. 53, 89–92.
Deenen, M.H.L., Langereis, C.G., van Hinsbergen, D.J.J., Biggin, A.J., 2011. Geomagnetic secular variation and the statistics of palaeomagnetic directions. Geophys. J. Int. 186, 509–520.
Diem, B., 1986. Die Untere Meeresmolasse zwischen der Saane (Westschweiz) und der Ammer (Oberbayern). Eclogae Geol. Helv. 79 (2), 493–559.
Dohmann, L., 1991. Die Unteroligozänen Fischschiefer im Molassebecken. Diss. Univ. München.
Doppler, G., Heissig, K., Reichenbacher, B., 2005. Die Gliederung des Tertiärs im süddeutschen Molassebecken. Newsl. Stratigr. 41, 359–375.
Egger, L.M., Śliwińska, K.K., Van Peer, T.E., Liebrand, D., Lippert, P.C., Friedrich, O., Wilson, P.A., Norris, R.D., Pross, J., 2016. Magnetostratigraphically-calibrated dinoflagellate cyst bioevents for the uppermost Eocene to lowermost Miocene of the western North Atlantic (IODP Expedition 342, Paleogene Newfoundland sediment drifts). Rev. Palaeobot. Palynol. 234, 159–185.
Ellwood, B., Crick, C., El Hassani, A., Benoist, S., Young, R., 2000. Magnetosusceptibility event and cyclostratigraphy method applied to marine rocks: detrital input versus carbonate productivity. Geology 28, 1135–1138.
Espitalié, J., LaPorte, J.L., Madec, M., Marquis, F., Leplat, P., Paulet, J., Boutefeu, A., 1977. Méthode rapide de characterisation des roches mères de leur potential pétrolier et de leur degree d'evolution. Rev. l'Institut Fr. du Pétrole. 32. pp. 23–42.
Fensome, R.A., 2004. The Lentin and Williams Index of Fossil Dinoflagellages (Contribution Series Number 42). Dallas, TX, American Association of Stratigraphic Palynologists Foundation.
Fisher, R., 1953. Dispersion on a sphere. Proc. R. Soc. Lond. 217, 295–305.
Georgiev, G., 2012. Geology and hydrocarbon systems in the Western Black sea. Turk. J. Earth Sci. 21, 723–754.
Gradstein, F.M., Ogg, J.G., Schmitz, M., 2012. The Geologic Time Scale 2012. Elsevier.
Hay, W.W., 1996. Tectonics and climate. Geol. Rundsch. 85, 409–437.
Hay, W.W., 1998. Detrital sediment fluxes from continents to oceans. Chem. Geol. 145, 287–323.
Hay, W.W., Mohler, H.P., Wade, M.E., 1966. Calcareous nannofossils from Nal'chik (northwest Caucasus). Eclogae Geol. Helv. 59, 379–399.
van Hinsbergen, D.J.J., 2004. The Evolving Anatomy of a Collapsing Orogen (PhD Thesis). Utrecht University (Geologica Ultraiectina).
Höfle, H.-C., Kuhnert, C., 1969. Erläuterungen zur Geologischen Karte von Bayern 1:25 000 Blatt Nr. 8331 Bayersoien.
Honjo, S., Roman, M.R., 1978. Marine copepod fecal pellets-production, preservation and sedimentation. J. Mar. Res. 36, 45–57.
Houben, A.J.P., van Mourik, C.A., Montanari, A., Coccioni, R., Brinkhuis, H., 2012. The Eocene-Oligocene transition: changes in sea level, temperature or both? Palaeogeogr. Palaeoclimatol. Palaeoecol. 335–336, 75–83.
Hudson, S.M., Johnson, C.L., Efendiyeva, M.A., Rowe, H.D., Feyzullayev, A.A., Aliyev, C.S., 2008. Stratigraphy and geochemical characterization of the Oligocene–Miocene Maikop series: implications for the paleogeography of Eastern Azerbaijan. Tectonophysics 451, 40–55.
Hüsing, S., Zachariasse, W.-J., van Hinsbergen, D.J.J., Krijgsman, W., Inceöz, M., Harzhauser, M., Mandic, O., Kroh, A., 2009. Oligocene–Miocene basin evolution in SE Anatolia, Turkey: constraints on the closure of the eastern Tethys gateway. Geol. Soc. Lond. Spec. Publ. 311, 107–132 (Collis. Collapse Africa-Arabia-Eurasia Subduction Zo).
Johnson, C.L., Hudson, S.M., Rowe, H.D., Efendiyeva, M.A., 2010. Geochemical constraints on the Palaeocene-Miocene evolution of eastern Azerbaijan, with implications for the South Caspian basin and eastern Paratethys. Basin Res. 22, 733–750.
Kempf, O., Matter, A., 1999. Magnetostratigraphy and depositional history of the Upper Freshwater Molasse (OSM) of eastern Switzerland. Eclogae Geol. Helv. 92, 97–103.
Kempf, O., Pross, J., 2005. The lower marine to lower freshwater Molasse transition in the northern Alpine foreland basin (Oligocene; central Switzerland-south Germany): age and geodynamic implications. Int. J. Earth Sci. 94, 160–171.

Kempf, O., Schlunegger, F., Strunck, P., Matter, A., 1998. Palaeomagnetic evidence for late Miocene rotation of the Swiss Alps: results from the north Alpine foreland basin. Terra Nova 10, 6–10.
Kirschvink, J.L., 1980. The least-squares line and plane and the analysis of palaeomagnetic data. Geophys. J. Int. 62, 699–718.
Koymans, M.R., Langereis, C.G., Pastor-Galán, D., van Hinsbergen, D.J.J., 2016. Paleomagnetism.org: an online multi-platform open source environment for paleomagnetic data analysis. Comput. Geosci. 93, 127–137.
Kuhlemann, J., Kempf, O., 2002. Post-Eocene evolution of the North Alpine Foreland Basin and its response to Alpine tectonics. Sediment. Geol. 152, 45–78.
Langereis, C.G., Krijgsman, W., Muttoni, G., Menning, M., 2010. Magnetostratigraphy – concepts, definitions, and applications. Newsl. Stratigr. 43, 207–233.
Laskarev, V., 1924. Sur les équivalents du sarmatien supérieur en Serbie, in: Receuil de Traveaux Offert À M. Jovan Cvijic Par Ses Amis et Collaborateurs a L'occasion de Ses Trente-Cinq Ans de Travail Scientifique.
Lemcke, K., 1983. Indications of a large eustatic sea-level fall at the Rupelian/Chattian boundary in the German Molasse Basin. Bull. Ver. Schweiz. Pet. Ing. 49, 57–60.
Lerche, I., Ali-Zadeh, A., Guliyev, I., Bagirov, E., Nadirov, R., Tagiyev, M., Feizullayev, A., 1997. South Caspian Basin: Stratigraphy, Geochemistry and Risk Analysis.
Martini, E., 1970. Standard Palaeogene calcareous nannoplankton zonation. Nature 226, 560–561.
Martini, E., 1971. Standard Tertiary and Quaternary calcareous nannoplankton zonation. In: Proceedings of the Second Planktonic Conference.
Maurer, H., Buchner, E., Seyfried, H., 2002. Wie marin is die Untere Meeresmolasse? Überlegungen zur Entstehung der Deutenhausener Schichten (basale Untere Meeresmolasse) im westlichen Oberbayern. Z. Dtsch. Geol. Ges. 153, 77–91.
McFadden, P.L., McElhinny, M.W., 1988. The combined analysis of remagnetization circles and direct observations in palaeomagnetism. Earth Planet. Sci. Lett. 87, 161–172.
Miller, K.G., Wright, J.D., Katz, M.E., Wade, B.S., Browning, J.V., Cramer, B.S., Rosenthal, Y., 2009. Climate threshold at the Eocene-Oligocene transition: Antarctic ice sheet influence on ocean circulation. Geol. Soc. Am. Spec. Pap. 452, 169–178.
Mullender, T.A.T., Velzen, A.J., Dekkers, M.J., 1993. Continuous drift correction and separate identification of ferrimagnetic and paramagnetic contributions in thermomagnetic runs. Geophys. J. Int. 114, 663–672.
Mullender, T.A.T., Frederichs, T., Hilgenfeldt, C., de Groot, L.V., Fabian, K., Dekkers, M.J., 2016. Automated paleomagnetic and rockmagnetic data acquisition with an in-line horizontal "2G" system. Geochem. Geophys. Geosyst. 17, 1–14.
Nadirov, R.S., Bagirov, E., Tagiyev, M., Lerche, I., 1997. Flexural plate subsidence, sedimentation rates, and structural development of the super-deep South Caspian Basin. Mar. Pet. Geol. 14, 383–400.
Okada, H., Bukry, D., 1980. Supplementary modification an introduction of code numbers to the low-latitude coccolith biostratigraphic zonation (Bukry, 1973; 1975). Mar. Micropaleontol. 5, 321–325.
Palcu, D., Popov, S.V., Golovina, L.A., Vernyhorova, Y.V., Krijgsman, W., n.d. The Shutdown of an Anoxic Sea-Giant. A Tectonic-Eustatic Interplay in the Time of the Middle Miocene Climatic Optimum.
Perch-Nielsen, K., 1985a. Mesozoic calcareous nannofossils. In: Perch-Nielsen, K. (Ed.), Plankton Stratigraphy. Cambridge University Press, pp. 329–426.
Perch-Nielsen, K., 1985b. Cenozoic calcareous nannofossils. In: Perch-Nielsen, K. (Ed.), Plankton Stratigraphy. Cambridge University Press, pp. 427–553.
Popov, S.V., Studencka, B., 2015. Brackish-water Solenovian mollusks from the Lower Oligocene of the Polish Carpathians. Paleontol. J. 49, 342–355.
Popov, S.V., Rögl, F., Rozanov, A.Y., Steininger, F.F., Shcherba, I.G., Kovac, M., 2004. Lithological-Paleogeographic maps of Paratethys - 1- maps Late Eocene to Pliocene. Courier Forschungs-Institut Senckenberg, Frankfurt am Main.
Popov, S.V., Sychevskaya, E.K., Akhmet'ev, M.A., Zaporozhets, N.I., Golovina, L.A., 2008. Stratigraphy of the Maikop Group and Pteropoda Beds in northern Azerbaijan. Stratigr. Geol. Correl. 16, 664–677.
Powell, A.J., 1992. Dinoflagellate cysts of the Tertiary System. In: A Stratigraphic Index of Dinoflagellate Cysts. Springer, Netherlands, pp. 155–251.
Premoli Silva, I., Jenkins, D.G., 1993. Decision on the Eocene–Oligocene boundary stratotype. Episodes 19, 379–382.
Pross, J., Houben, A.J.P., van Simaeys, S., Williams, G.L., Kotthoff, U., Coccioni, R., Wilpshaar, M., Brinkhuis, H., 2010. Umbria-Marche revisited: a refined magnetostratigraphic calibration of dinoflagellate cyst events for the Oligocene of the Western Tethys. Rev. Palaeobot. Palynol. 158, 213–235.
Reichenbacher, B., Uhlig, U., Kowalke, T., Bassler, B., Matzke-karasz, R., Schenk, B., 2004. Biota, palaeoenvironments and biostratigraphy of continental Oligocene deposits of the South German Molasse Basin (Penzberg Syncline). Paleontology 47, 639–677.
Rögl, F., 1998. Palaeogeographic considerations for Mediterranean and Paratethys Seaways (Oligocene to Miocene). Ann. Naturhist. Mus. Wien 99, 279–310.
Rögl, F., 1999. Mediterranean and paratethys. Facts and hypotheses of an Oligocene to Miocene paleogeography (short overview). Geol. Carpath. 50, 339–349.
Sachsenhofer, R.F., Schulz, H-M., 2006. Architecture of Lower Oligocene source rocks in the Alpine Foreland Basin: a model for syn-and post-depositional source-rock features in the Paratethyan realm. Pet. Geosci. 12 (4), 363–377.
Sachsenhofer, R.F., Popov, S.V., Akhmetiev, M.A., Bechtel, A., Gratzer, R., Groß, D., Horsfield, B., Rachetti, A., Rupprecht, B., Schaffar, W.B.H., Zaporozhets, N.I., 2017. The type section of the Maikop Group (Oligocene–lower Miocene) at the Belaya River (North Caucasus): depositional environment and hydrocarbon potential. Am. Assoc. Pet. Geol. Bull. 101 (3), 289–319.
Schlunegger, F., Castelltort, S., 2016. Immediate and delayed signal of slab breakoff in Oligo/Miocene Molasse deposits from the European Alps. Sci. Rep. 6, 1–11.
Schlunegger, F., Kissling, E., 2015. Slab rollback orogeny in the Alps and evolution of the Swiss Molasse basin. Nat. Commun. 6, 8605.
Schlunegger, F., Rieke-Zapp, D., Ramseyer, K., 2007. Possible environmental effects on the evolution of the Alps-Molasse Basin system. Swiss J. Geosci. 100, 383–405.
Schmiedl, G., Scherbacher, M., Bruch, A., Jelen, B., Nebelsick, J., Hemleben, C., Mosbrugger, V., Rifelj, H., 2002. Paleoenvironmental evolution of the Paratethys in the Slovenian Basin during the Late Paleogene. Int. J. Earth Sci. 91, 123–132.
Schulz, H.-M., Sachsenhofer, R.F., Bechtel, A., Polesny, H., Wagner, L., 2002. The origin of hydrocarbon source rocks in the Austrian Molasse Basin (Eocene–Oligocene transition). Mar. Pet. Geol. 19, 683–709.
Schulz, H., Bechtel, A., Sachsenhofer, R.F., 2005. The birth of the Paratethys during the Early Oligocene: from Tethys to an ancient Black Sea analogue? Glob. Planet. Chang. 49, 163–176.
Sissingh, W., 1998. Comparative Tertiary stratigraphy of the Rhine Graben, Bresse Graben and Molasse Basin: correlation of Alpine foreland events. Tectonophysics 300, 249–284.
Sissingh, W., 2001. Tectonostratigraphy of the West Alpine Foreland: correlation of Tertiary sedimentary sequences, changes in eustatic sea-level and stress regimes. Tectonophysics 333, 361–400.
Sissingh, W., 2006. Syn-kinematic palaeogeographic evolution of the West European Platform: correlation with Alpine plate collision and foreland deformation. Neth. J. Geosci. 85, 131–180.
Stauner, M., Leitner, C., Gross, D., 2015. Organisches Material an der Ammer bei Scheibum (Bausteinschichten, Molasse). Jahrb. Geol. Bundesanst. 155, 97–108.
Tagiyev, M.F., Nadirov, R.S., Bagirov, E.B., Lerche, I., 1997. Geohistory, thermal history and hydrocarbon generation history of the north-west South Caspian basin. Mar. Pet. Geol. 14, 363–382.
Tauxe, L., Kent, D., 2004. A simplified statistical model for the geomagnetic field and the detection of shallow bias in paleomagnetic inclinations: was the ancient magnetic field dipolar. In: Timescales Paleomagn. Field. 145. pp. 101–115.
Tauxe, L., Butler, R.F., Van der Voo, R., Banerjee, S.K., 2010. Essentials of Paleomagnetism. University of California Press, California.
Torsvik, T.H., Van der Voo, R., Preeden, U., Niocaill, C. Mac, Steinberger, B., Doubrovine, P.V., van Hinsbergen, D.J.J., Domeier, M., Gaina, C., Tohver, E., Meert, J.G., McCausland, P.J.A., Cocks, L.R.M., 2012. Phanerozoic polar wander, palaeogeography and dynamics. Earth Sci. Rev. 114, 325–368.
Van Simaeys, S., Munsterman, D., Brinkhuis, H., 2005. Oligocene dinoflagellate cyst biostratigraphy of the southern North Sea Basin. Rev. Palaeobot. Palynol. 134, 105–128.
Van Velzen, A.J., Zijderveld, J.D.A., 1995. Effects of weathering on single-domain magnetite in Early Pliocene marine marls. Geophys. J. Int. 121, 267–278.
Varol, O., 1999. Paleogene. In: Bown, P.R. (Ed.), Calcareous Nannofossil Biostratigraphy. Kluwer Academic Publishing, Dordrecht/Boston/London, pp. 201–224.
Vasiliev, I., Krijgsman, W., Langereis, C.G., Panaiotu, C.E., Maţenco, L., Bertotti, G., 2004. Towards an astrochronological framework for the eastern Paratethys Mio-Pliocene sedimentary sequences of the Focşani basin (Romania). Earth Planet. Sci. Lett. 227, 231–247.
Verhallen, P.J.J.M., Romein, A.J.T., 1983. Calcareous nannofossils from the Priabonian stratotype and correlations with the parastratotypes. Utrecht Micropaleontol. Bull. 29, 163–173.
Vincent, S.J., Allen, M.B., Ismail-Zadeh, A.D., Flecker, R., Foland, K.A., Simmons, M.D., 2005. Insights from the Talysh of Azerbaijan into the Paleogene evolution of the South Caspian region. Geol. Soc. Am. Bull. 117, 1513–1533.
Wessely, G., 1987. Mesozoic and Tertiary evolution of the Alpine-Carpathian foreland in eastern Austria. Tectonophysics 137, 45–59.
Williams, G.L., Brinkhuis, H., Pearce, M.A., Fensome, R.A., Weegink, J.W., 2004. Southern Ocean and global dinoflagellate cyst events compared: index events for the Late Cretaceous–Neogene. Proc. Ocean Drill. Program Sci. Results 189.
Zijderveld, J.D.A., 1967. AC demagnetization of rocks: analysis of results. In: Collinson, D.W., Creer, K.M. (Eds.), Methods in Paleomagnetism. Elsevier, Amsterdam, pp. 254–286.